5. Synoptic-scale Phenomena

5.1. Front Analysis

5.1.1. Concept of Fronts

Fronts are defined as boundaries between air masses, with clouds emerging when vertical circulation is active at divisions between areas with different densities. Belt-form cloud bands are observed in the vicinity of fronts on a synoptic scale, providing a starting point for front analysis in satellite imagery. Cases in which no clouds form with vertical circulation are occasionally seen over dry continental areas, with only a band consisting of upper cloud carried by strong winds in the upper troposphere. It should therefore be noted that fronts cannot be identified from cloud bands alone.

To highlight the structure of disturbances, Browning (1990) proposed the concepts of warm conveyor belts (WCBs) and cold conveyor belts (CCBs) in reference to major atmospheric currents on a coordinate system relative to the disturbance. The WCB and CCB concepts were also adopted by Carlson (1980) to clarify cyclonic and frontal structures (Fig. 5-1-1).

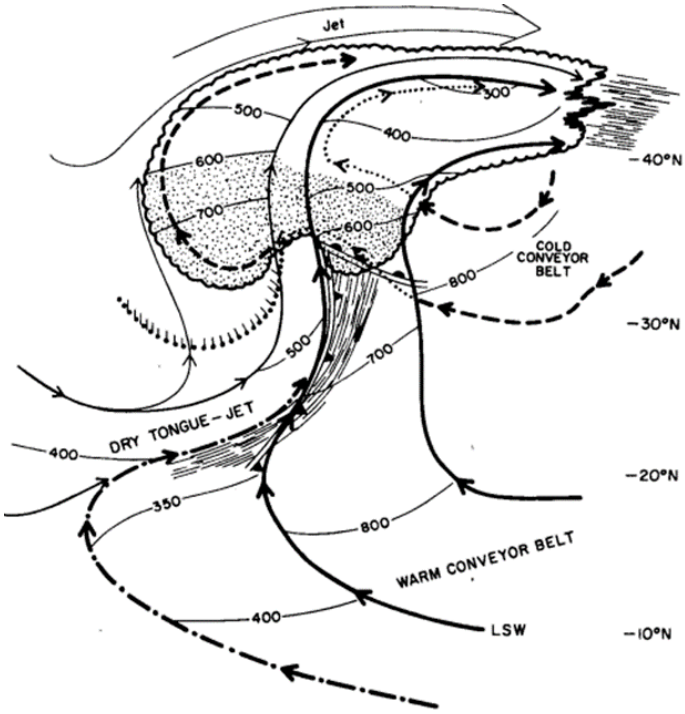

Fig. 5-1-1. Conveyor belt model (Carlson (1980), with open-arrow addition). Solid lines: WCB; dashed lines: CCB; numbers: current altitudes; dash-dots: low cloud edge

WCB currents carry warm wet air upward, contributing significantly to cloud formation. This creates southeastern winds in the lower layer at the edge of anticyclones, ascending northward in warm cyclone areas and gradually changing direction clockwise. These currents are associated with warm advection ahead of troughs. Cloud emerges when WCBs reach

condensation level, with a cloud top height directly proportional to the distance of northern shift. WCBs meeting an upper-jet axis change direction eastward as northward ascension is suppressed.

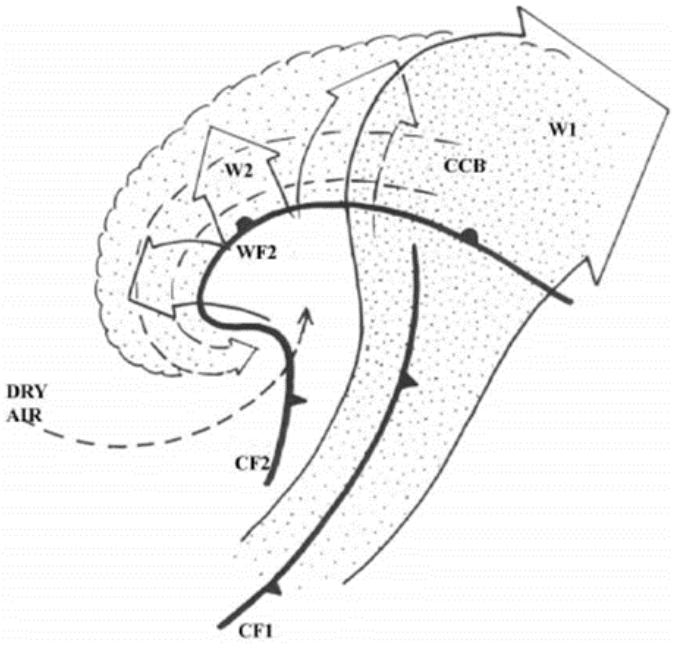

Fig. 5-1-2. Secondary WCB model (Browning, 2004)
W1: WCB; W2: secondary WCB

CCBs are currents located toward the cyclonic center, moving in parallel to the frontal side of a warm front. In satellite imagery, they are recognized as lower cloud and progress westward, moving under WCBs. This makes them unrecognizable by satellites, but they cross WCBs at a large angle at the western edge of the WCB cloud band, thereby manifesting as middle- and low-cloud areas extending westward. Along with such extension, part of the cloud mass rises, creating anticyclonic currents with subsequent eastward movement at jet-stream altitude. Other parts move with no height change toward the cyclonic center along with cyclonic currents, maintaining middle- and low-cloud status (bold open arrows in Fig. 5-1-2). Among CCB types, Bader *et al.* defined secondary WCBs (referred to here as W2s) as currents that assume anticyclonic curvature as they ascend (Fig. 5-1-2).

W2s are thought to develop under WCB conditions from updraft ahead of short-wave troughs. In the definition of Bader *et al.*, the term CCB refers specifically to currents at lower altitudes moving toward the cyclonic center.

Figure 5-1-3 shows a conveyor belt formation in infrared imagery, with the cloud area **W-W** associated with a WCB. The **W-W** cloud top is higher in the north, and a stratified cloud area is seen. This area appears to consist of thicker clouds than in visible imagery. The eastern terminal of the cloud area **E** consists of thin Ci, indicating that the upper clouds in the WCB formation turned eastward with jet-stream axis encounter. The **C1-C2-C3** cloud band is associated with a CCB. As the clouds around **C1** move above the CCB, many upper clouds are

seen. The CCB is below the WCB, making it unrecognizable in satellite imagery. This is seen as a protrusion to the west of the WCB cloud band around **C2**. The **C2-C3** cloud top rises with westward progression, and the mass then joins the WCB upon turning eastward as it encounters the jet axis. A current diverted from the CCB is also seen entering the cyclonic circulation (from **C2** to **d**), maintaining a low cloud top.

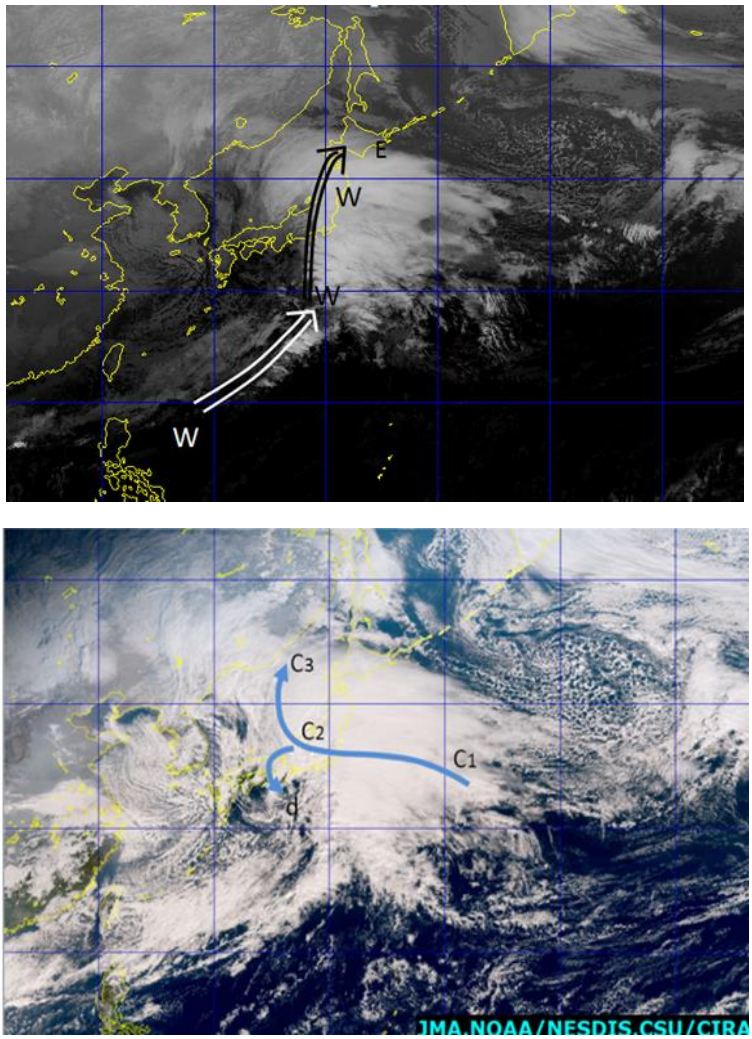

Fig. 5-1-3. Conveyor belt at 00:00 UTC on 18 January 2016
Top: B13 infrared image (arrow: WCB)
Bottom: True Color Reproduction image (arrow: CCB)

5.1.2. Warm Fronts

Warm fronts form at the boundaries of warm-air masses migrating along and creeping over cold-air masses, such as WCBs gliding over CCBs. These are observed as boundaries of WCB currents ascending northward from warm areas and beginning to slide over cold CCBs flowing toward a cyclonic center. This corresponds to the southern rim of stratiform cloud formations among currents along WCBs. In addition to stratiform clouds, convective clouds are also present near the front, as reported by Neiman (1993) with an elevator-escalator model illustrating mesoscale convective clouds around a CCB-WCB cross-point (Fig. 5-1-4).

In this model construction, warm fronts can be identified from satellite imagery in correspondence to the southern edge of cloud areas containing convective clouds. However, it is often difficult to determine the southern edge of cloud areas associated with warm fronts due to cloud development in warm areas and coverage by upper and middle clouds. Accordingly, identifying warm fronts in satellite imagery can be challenging. CCB formation is often minimal in the early cyclonic phase or in comma-style cyclones (see below), making lower clouds along warms front unclear.

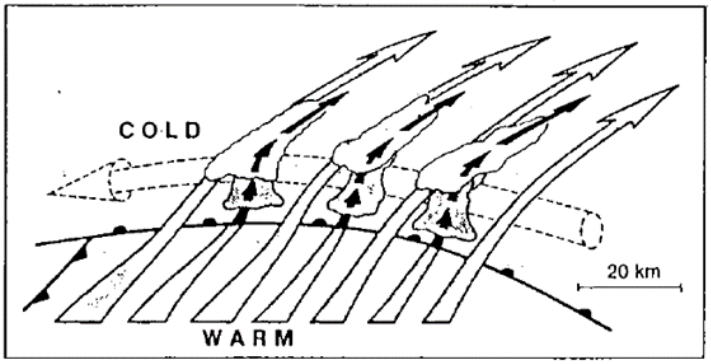

Fig. 5-1-4. Elevator-escalator model (Neiman, 1993)
Dashed lines: CCB; open arrows: WCB (escalator); black dots: clouds; black arrows: ascending currents associated with mesoscale convection (elevator)

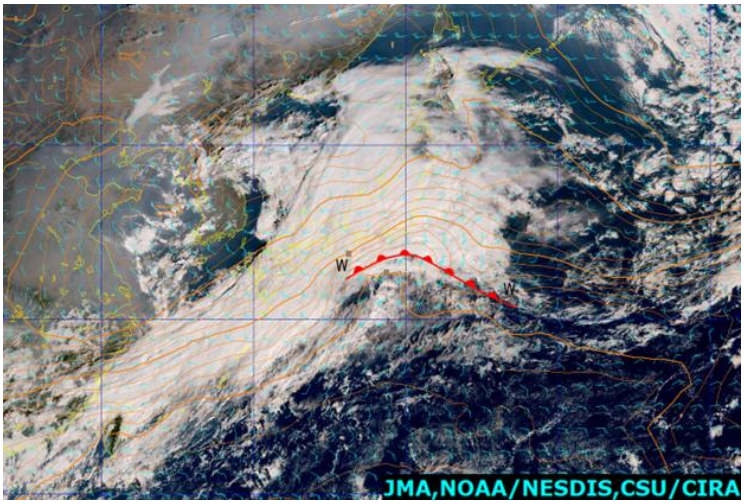

Fig. 5-1-5. Warm-front analysis for 00:00 UTC on 2 November 2015
True Color Reproduction image and objective analysis for 850 hPa (temperature, wind)

Figure 5-1-5 presents a simple case of warm front determination, with a cloud area along a cyclone between the Tokai and Kanto regions. The southern rim of the cloud area **W-W** is distinct, with convective cloud lines and a northern part consisting of upper and middle clouds. In satellite imagery, a warm front is observed along the southern rim, corresponding to a 12°C isotherm at 850 hPa based on objective analysis.

Warm fronts can be identified when lower cloud along a warm front is obscure, as when cold air regions are identified from cloud patterns within cold air fields ahead of a cyclone, or with estimation of wind direction from low-cloud movement. The dashed line in Fig. 5-1-6 indicates the estimated southern limit of a lower cold-air region behind the developed cyclone. The low cloud area **W-W** is seen westward of this line. A warm front associated with a cyclone passing near Japan is identified from the cloud area around **W-W** progressing eastward overall and from individual clouds migrating northwestward, enabling identification of a southeastward wind field ahead of the warm front.

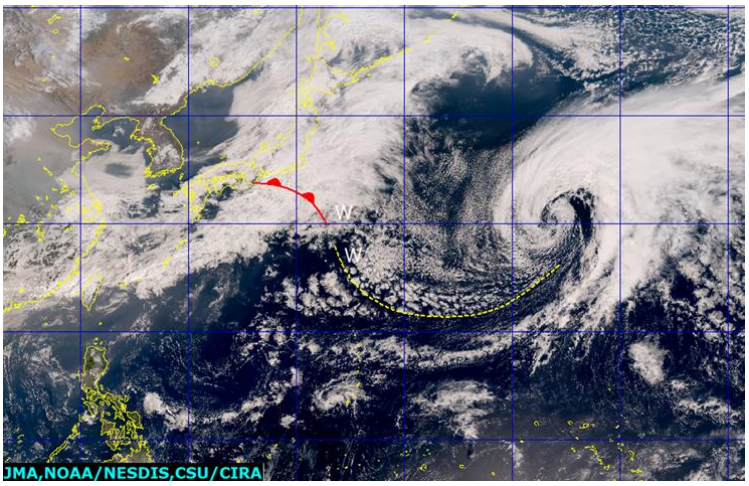

Fig. 5-1-6. Challenging warm-front analysis
True-Color Reproduction image for 00:00 UTC on 19 March 2016

5.1.3. Cold Fronts

Cold fronts may be Ana-type (associated with extreme weather changes near fronts) or Kata-type (associated with milder weather changes). Ana fronts are the textbook type, often featuring in cold-front analysis, but the Kata type is also common. The characteristics of each type in satellite imagery are described below, along with notable key features in cold-front analysis.

5.1.3.1. Ana Cold Fronts

Ana-type cold fronts are categorized as rearward-ascending types in the WCB model described by Browning (1990; Fig. 5-1-7). They are associated with inflows of intense cold air with a WCB inclined rearward, with an intense updraft arising in association with the cold front and warm air ascending relatively gently toward its rear. The band comprising the front features convective line cloud convection in a narrow part of the front edge alongside warm air, and the rear edge of the band consists of stratiform clouds. In satellite imagery, cloud bands corresponding to the Ana type have an aligned convective structure on the warm-air side, and the position of the cold front corresponds to convective cloud lines at the front of the band. Over sea areas during cold periods, cell-form convective clouds develop in association with cold-air inflow at the rear of the front, allowing identification of Ana-type forms from this cloud

presence and related activity.

In Fig. 5-1-8, a cloud band is seen extending southwestward from a cyclone south of the Kamchatka Peninsula. At its southeastern edge (i.e., the warm-air side), active convective clouds align along **C-C**, allowing identification of the band as the Ana type. The position of the cold front can be estimated to be along **C-C**.

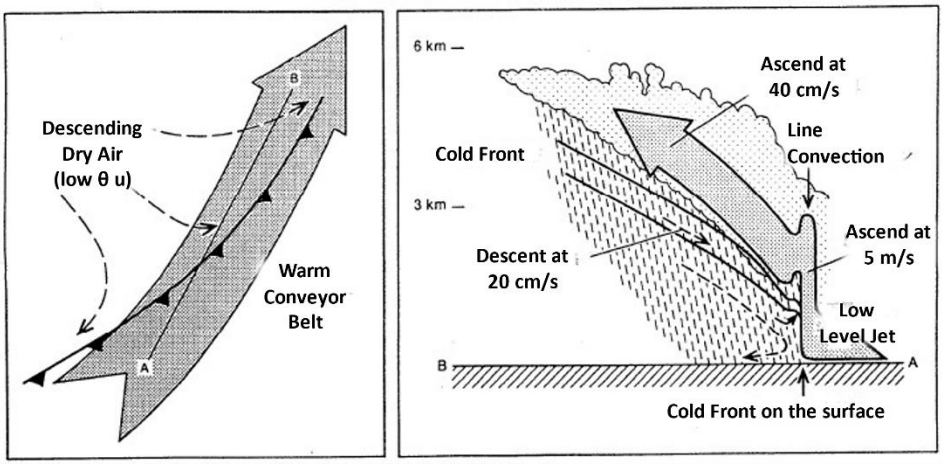

Fig. 5-1-7. Flows in a typical Ana cold front (from Kitabatake *et al.*, 1995)
Open arrow: rearward ascending WCB at the cold front under descending cold air (dashed lines)
Left: plane view; right: section along **A-B** in the diagram on the right

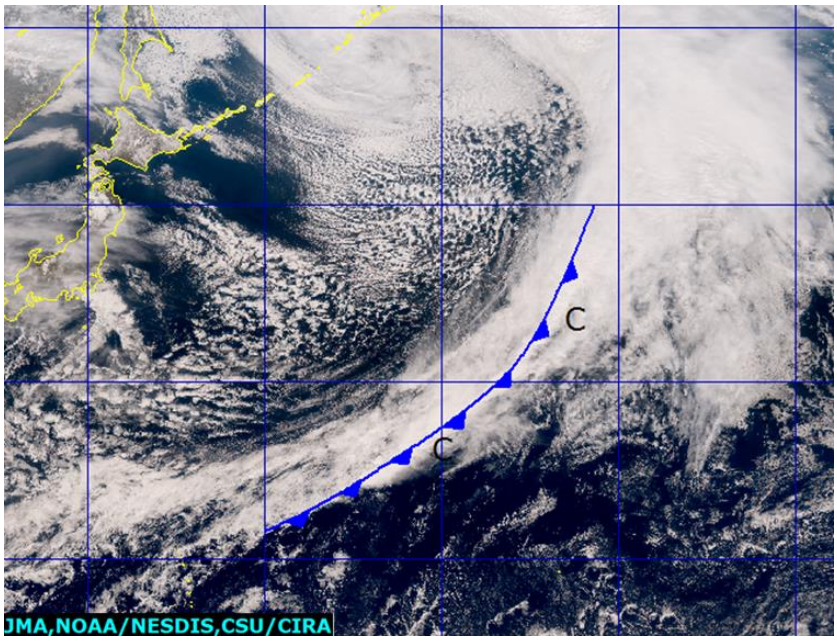

Fig. 5-1-8. An Ana cold front at 00:00 UTC on 16 March 2016
True Color Reproduction image indicating cold-front position (see the main text for alphabetical designations)

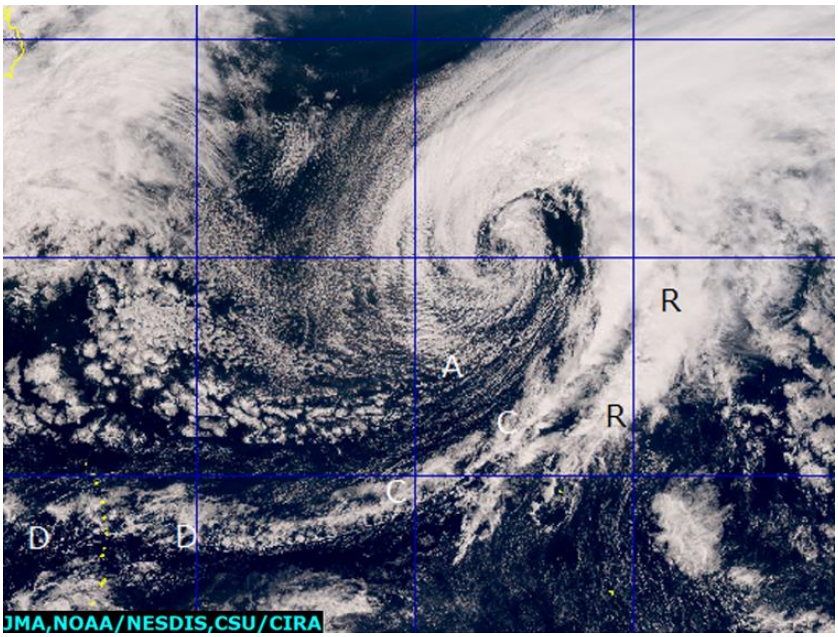

Fig. 5-1-9. An Ana cold front at 00:00 UTC on 19 March 2016
True Color Reproduction image indicating cold-front position (see the main text for alphabetical designations)

In Fig. 5-1-9, a rope cloud formation marked by **C-C** is seen at the front edge of the cloud band. Rope clouds are often observed at the advancing front edge of cloud bands extending from cyclones at maturity or during dissipation. A cold front can be determined at the position of the rope cloud in this case. Although the cloud area **D-D** is also present west of **C-C**, this is not considered to correspond to the cold front as it is distant from the cloud band and discontinuous. A cell-form convective cloud formation marked **A** is seen over the sea at the rear of the front in association with strong cold advection. The active convective cloud band **R-R** is also seen with a 100 – 200 km width in front of the rope cloud, representing a rain band within the warm area. As such bands are often seen in warm areas, care should be taken to avoid misidentification as cold fronts.

5.1.3.2. Kata Cold Fronts

Kata-type cold fronts are categorized as forward-ascending types in the WCB model described by Browning (1990; Fig. 5-1-10). Upper cold fronts (UCFs) may emerge when dry air with a low equivalent potential temperature descends from the upper atmosphere and overtakes the surface cold front, thereby initiating convective instability between the WCB beneath and warm wet air within warm areas, increasing the likelihood of rain band development that may bring extreme phenomena such as intense rainfall and gusting winds. Shallow moist zones (SMZs) consisting of low convective clouds with light rain may be present between rain bands and surface cold fronts. Such Kata formations are known as split fronts.

Changes in Kata cold-front weather accompanying surface cold-front passage are limited in

comparison to those of rain-band passage. Rain bands and UCFs are clearly recognizable in satellite imagery, while identification of surface cold fronts comprising lower clouds with coarser organization is more challenging.

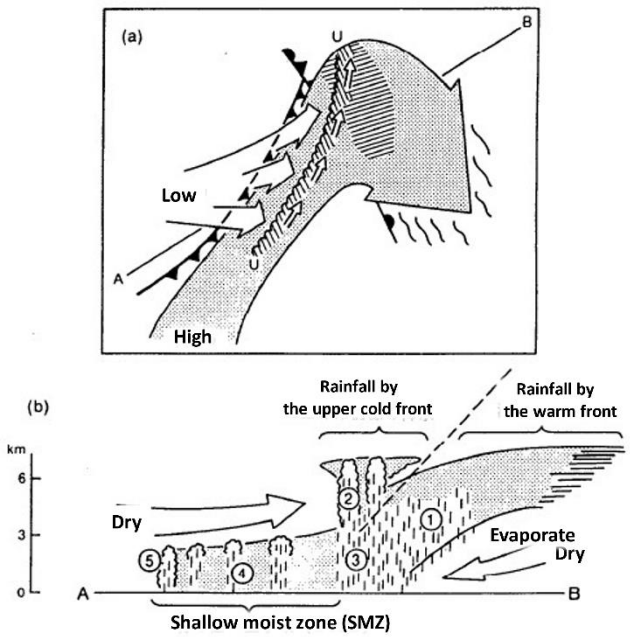

Fig. 5-1-10. Kata cold front (split front) (Kitabatake *et al.*, 1995)
(a): plane view, with open dotted arrows representing forward-type WCB forms and open arrows representing dry air; (b): section view of (a) along **A-B** 1.: rainfall from warm front; 2.: upper cell generating convective precipitation with UCF (indicated by **U-U** in (a)); 3.: rainfall from UCF; 4.: shallow moist zone (SMZ) between UCF and surface cold front; 5.: shallow precipitation from cold front

In Fig. 5-1-11, a cloud band is seen extending southwestward from a cyclone east of Hokkaido. The tall convective cloud **A-A** corresponds to a surface cold front, which in turn corresponds to the western edge of a low cloud area (**B**, with a cloud top height under 700 hPa) to the west of **A-A**, as seen by the entry position of warm air and a concentration zone with an equivalent potential temperature at 850 hPa. In the vertical section view, the upper layer above 700 hPa is dry over the surface cold front, suppressing the top of the cloud area **B-B** with dry air. This dry air is a characteristic of Kata cold fronts, overtaking the surface cold front with intense southwestern winds in the middle and upper layers. A split-front structure is indicated by the correspondences of **A-A** to UCF conditions and **B-B** to SMZ conditions.

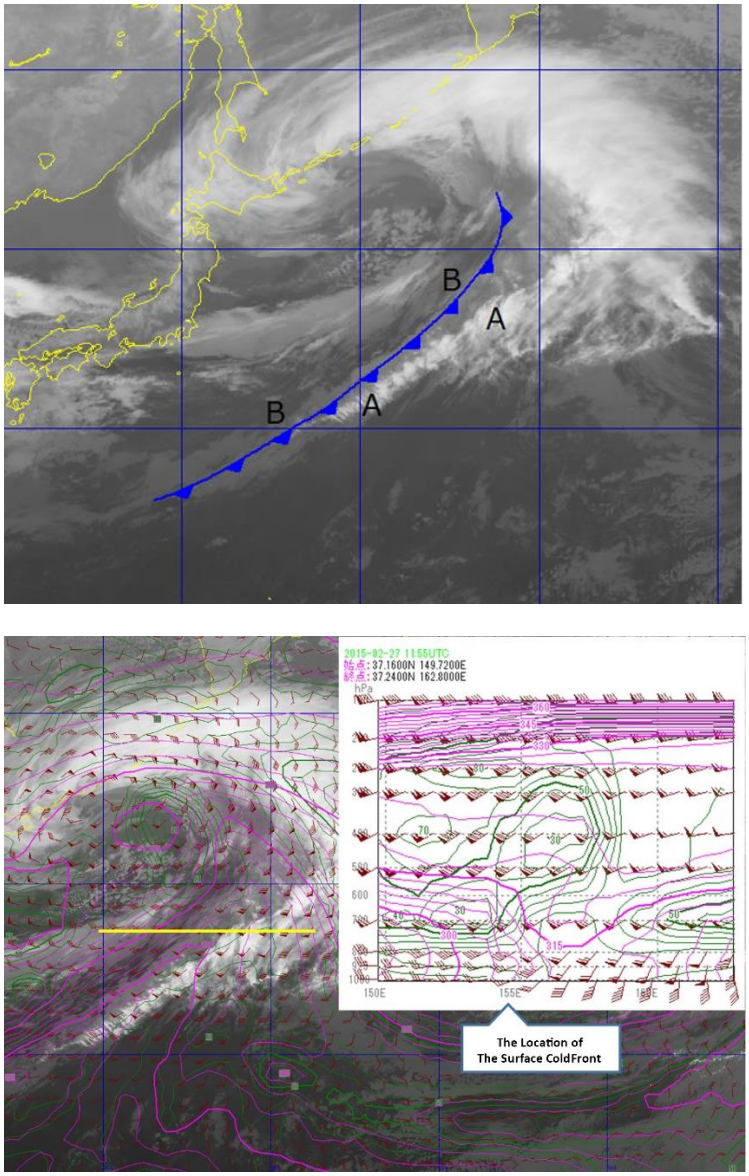

Fig. 5-1-11. A Kata cold front at 12:00 UTC on 27 February 2015
Top: B13 infrared image with a surface cold front; bottom: B13 infrared image with 850-hPa equivalent potential temperature, humidity and a vertical section view for the yellow latitudinal line. Pink: equivalent potential temperature; green: humidity; brown: wind

5.1.3.3. Points to Note Regarding Analysis

The points below regarding cold-front analysis should be noted (Fig. 5-1-12).

1. Even single cold fronts may exhibit a Kata-type structure near the cyclonic center due to dry-air descent from the upper atmosphere or an Ana-type structure away from the cyclonic center. Cyclones tend to be associated with such characteristics after the development stage. Hence, cold fronts associated with developing cyclones are generally located at the western edge of a cloud band (open arrows in the figure) and the southern edge of a cloud band (black arrows in the figure) at a distance.

2. In Ana-type structures, the front is identified as the position of a rope cloud formation. However, care should be taken in analysis of multiple rope cloud formations and fronts without cloud bands, which appear similar to convective cloud lines in warm areas and elsewhere.
3. Prominent convective clouds in warm areas may merge with cold fronts along marginal currents of anticyclones in a linear structure (e.g., cloud **A** in the figure), and may cause cold-front misidentification. In such cases, convective cloud lines in warm areas can be categorized by whether they pursue an anticyclonic path or have an anticyclonic curvature.

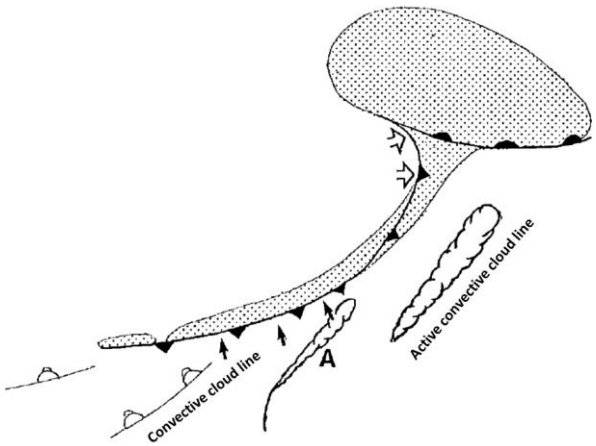

Fig. 5-1-12. Points of focus in cold-front determination
Dotted area: cloud; bold line: convective cloud; cloud areas: active convective cloud line (see the main text for a description of **A**)

5.1.4. Occluded Fronts

As shown in Fig. 5-1-13, occlusions can be either cold (man (人) type) or warm (lambda (λ) type). Discrimination is based on the temperature field and cloud patterns.

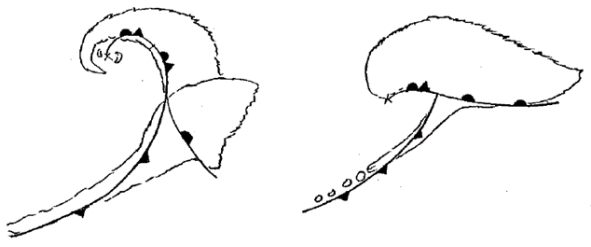

Fig. 5-1-13. Left: cold-occluded model (man (人) type); right: warm-occluded model (lambda (λ) type)

5.1.4.1. Decision-making on Occlusion Points

Saito (1979) identified the characteristics of occlusions (disappearances of warm areas in a cyclonic zone from the ground surface) as follows:

- A significant fall in air pressure

- A rapid decrease in phase differences between an 500-hPa trough and a cyclone on the ground
- A single pressure valley or a single shear current at 850 hPa or on the ground
- A wedge-shaped upper warm air mass immediately above or slightly ahead of a surface trough with no simultaneous increase in the surrounding temperature gradient
- An upper strong wind zone to the south outside the cyclonic center on the ground

Among these characteristics, the position of a strong wind zone can be determined in satellite imagery, and its axis can be estimated from Ci streaks in infrared imagery and boundaries in water vapor imagery. Fronts can also be identified from indicators such as frontal cloud bands largely parallel to the strong wind axis and cloud bands corresponding to CCB extending to the polar side across the frontal cloud band.

The general procedure for determination of occlusion points is outlined below, with reference to Fig. 5-1-14.

1. Strong-wind axis determination

   A strong wind axis is seen along a boundary corresponding to a jet stream at **J-J** in the water vapor image.

2. Cold-front determination

   In both visible and infrared imagery, a clear cloud band with a width of 200 – 400 km corresponding to a cold front is seen along **B-B**.

3. Warm-front determination

   In visible imagery, **W1-O-W2** is a cloud band equivalent to a CCB, corresponding to a warm front to the east of the cold frontal cloud band **W1-O**. This crosses the cold band, extending to the polar side **O-W2**. The imagery shows a clear CCB formation.

4. Occlusion point/occluded front determination

   An occlusion point is observed around the cross point **O** of the southern edge **W1-W2** at the warm side of a CCB and the boundary **J-J** corresponding to a jet stream. The cloud area **A** with a high top advances eastward from the occlusion point. This pattern tends to develop after the occlusion progresses toward dissipation. The cloud band **O-W2** associated with the CCB extends westward from the polar side of the cold frontal cloud band **B-B.** Below this, the southern edge of the low cloud corresponds to the occluded front.

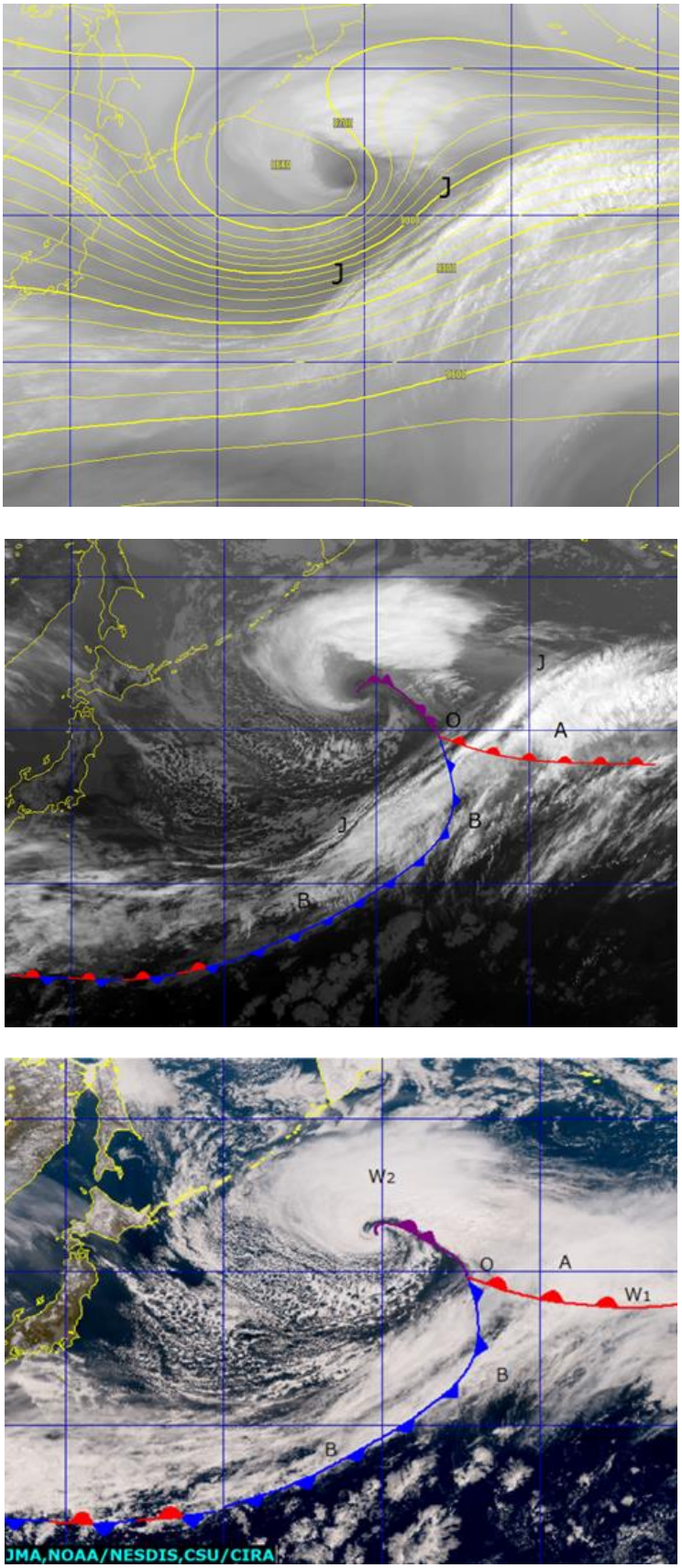

Fig. 5-1-14. Occlusion front at 00:00 UTC on 12 April 2016
Top: B10 water vapor image with 300-hPa isohypse; middle: B13 infrared image; bottom: True Color Reproduction image (see the main text for alphabetical designations)

5.1.4.2. Cold Occlusions

Cold occlusions often accompany developing cyclones ahead of a trough with intense cold air descending southward from the polar side. Characteristics of cold occlusions in satellite imagery include formation of comma-form clouds with latitudinal extension, weak warm fronts despite obvious cloud bands corresponding to cold fronts, cell-form or streaky convective clouds to the rear of a cyclone associated with intense cold air, and clear dry slots. However, the structure of warm fronts remains largely unclear; with obscure CCB conditions, occlusion point identification is challenging.

The cyclone around Sakhalin in Fig. 5-1-15 can be identified as a cold occlusion due to characteristics such as comma-shaped clouds, the streaky cloud area **B** at the rear of the cyclone in association with cold air, and a dry slot intertwining with the center. A jet axis is present along the boundary **J-J** in the water vapor image. Although warm fronts are hard to determine with minimal low-cloud scatter, such a front can be identified here from cell-form cloud area movement (around **W-W**) corresponding to the current around the anticyclone edge.

In this example, the cell-form cloud associated with the warm area heads northward, and northwestward around W-W. The cold front corresponds to the cloud band **C-C**. An occlusion point **O** is seen around the intersection of the cold frontal cloud band **C-C** and the warm frontal low cloud line **W-W**, and around the intersection of **J-J** for the upper strong-wind axis and **W-W**. Upper dry air forming a dry slot (seen as a dark area in the water vapor image) passes north of the occlusion point and is engulfed into the cyclonic center. Here, the dry slot overtakes the occlusion point, moving farther northward.

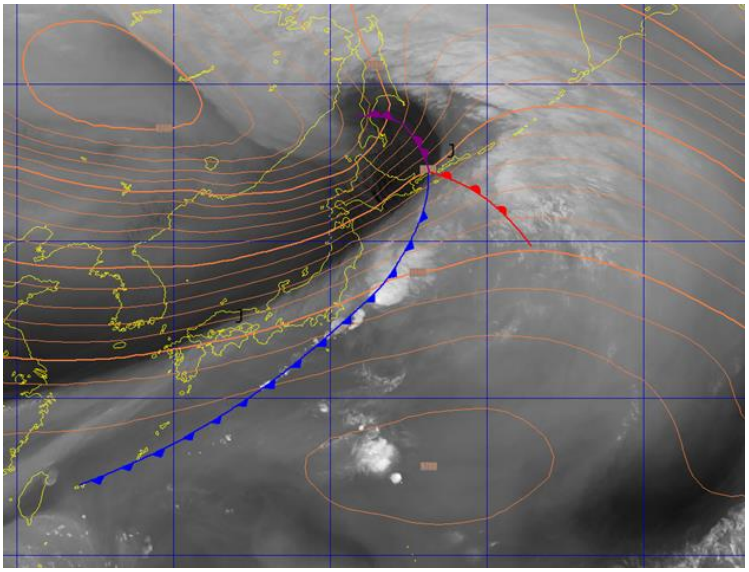

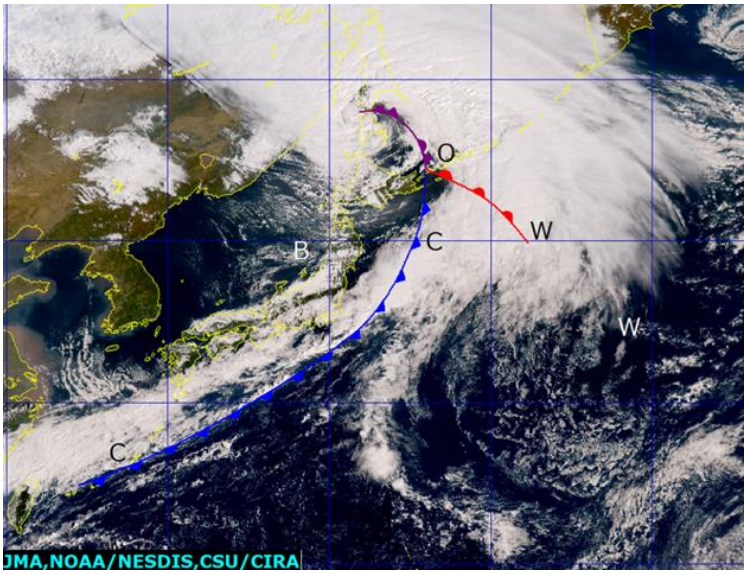

Fig. 5-1-15. A cold occlusion at 00:00 UTC on 2 October 2015
Top: B10 water vapor image, 300-hPa isohypse; bottom: True Color Reproduction image (see the main text for alphabetical designations)

5.1.4.3. Warm Occlusions

Warm occlusions correspond to inflow of weak cold air from the rear of cyclones. In satellite imagery, visible characteristics include λ-shaped or T-shaped cloud formations with a longitudinal strike, more distinct cloud bands corresponding to warm fronts than with cold occlusion, frequent obscuring of dry slots, and cell-form clouds accompanying cold air appearing obscure with limited extension at the rear of cyclones. Cold fronts can be either active or inactive. These characteristics contrast with those of cold occlusions, indicating the absence of intense cold-air inflow.

The cyclone to the east of Japan in Fig. 5-1-16 appears as a warm occlusion based on a λ form cloud pattern and unseen cell-form clouds with a clear area at the rear of the cyclone. In the water vapor image, a jet axis is seen along the boundary **J-J.** An occlusion point is observed at the intersection of the jet axis and a cloud band extending from northwest to southeast. The occlusion front extends to the occlusion point along the southern edge of a cloud band running from the cyclonic center **L**. A cloud area corresponding to a warm front is seen at **W-W**, with a stationary front to the east of the extension corresponding to the air mass boundary. The convective cloud line **C-C** corresponding to a cold front is clearly visible, albeit with weak activity.

The boundary corresponding to the jet here was relatively distinct, but the boundaries in the warm occlusion tended to be obscure. Occlusion points are also determined from the intersection of the cold and warm fronts.

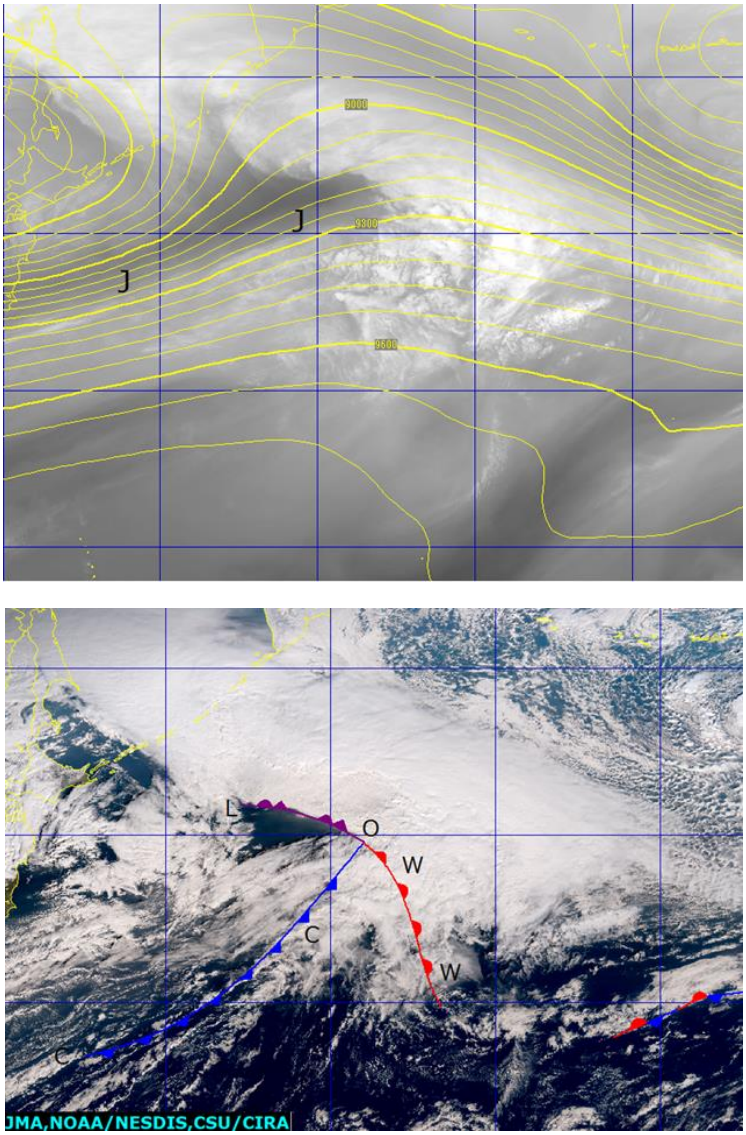

Fig. 5-1-16. An warm occlusion at 00:00 UTC on 4 December 2015
Top: B10 water vapor image, 300-hPa isohypse; bottom: True Color Reproduction image (see the main text for alphabetical designations)

5.1.5. Stationary Fronts

Movement perpendicular to the extension axis is limited in stationary fronts, and such forms are recognized as cloud bands stretching several thousand kilometers in satellite imagery. Mesoscale cyclones and frontal kinks in such fronts appear as active convective cloud band forms or cloud areas extending to the polar side with anticyclonic curvature on the northern edge.

Stationary fronts during cold periods frequently form long wide cloud bands, often with limited convective activity. Conversely, those during warm periods tend to be accompanied by active convective clouds along an inflow of warm wet air from the south, typically associated with the Baiu rain front and the autumn rain front.

5.1.5.1. Stationary Fronts during Cold Periods

During cold periods, stationary fronts often exhibit cloud bands connecting to a cold front extending from a developed cyclone. Such forms run parallel to the upper jet axis, presenting as long cloud bands with widths of 500 – 1,000 km and lengths of several thousand kilometers. These mainly consist of upper and middle clouds, with limited activity except at the southern edge. Stationary fronts on the ground are seen at the southern edge of cloud bands at 5 – 10° south latitude from the upper jet axis corresponding to the northern edge of the cloud band.

Figure 5-1-17 shows a stationary front during a cold period. Far east of Japan, a cold front accompanying a cyclone connected with a stationary front extends farther to the south of Okinawa. In B10 water vapor images, the dark area **B-B** corresponding to the upper jet stream is parallel to a cloud band at its northern edge. This band, with a 500 – 800 km width, consists mainly of upper and middle clouds and has no active convective clouds. Rain (0 – 1 mm per hour) was observed from stratiform clouds in the band over Okinawa. A stationary front is observed at the southern edge of the band. In surface observation, no notable change was seen for wind and temperature across the cloud band. The surface front was positioned at 7° south latitude from the jet axis. The gradient of the frontal surface was under 1/100, which was slightly steeper than a typical warm frontal surface (analysis by section at 35 degrees indicates a frontal surface gradient of 4.5 x 500 km).

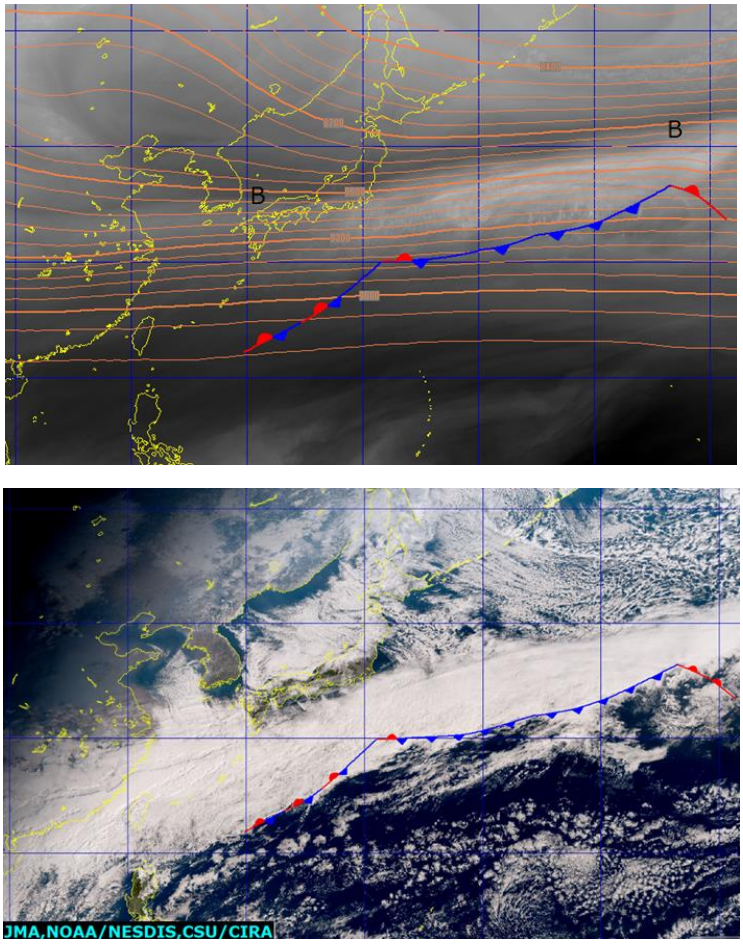

Fig. 5-1-17. A stationary front during a cold period at 00:00 UTC on 2 February 2016 Top: B10 water vapor image with 300-hPa isohypse; bottom: True Color Reproduction image (see the main text for alphabetical designations)

5.1.5.2. Stationary Fronts during Warm Periods

The Baiu rain front is a typical stationary formation that emerges around Japan during warm periods. It characteristically shows water vapor content with a larger gradient than that of temperature. It is narrower than stationary fronts observed during cold periods, appearing as a band mostly of convective clouds.

Figure 5-1-18 shows a Baiu front with a 100-km-wide cloud band, mostly consisting of middle and lower layers with active convection, extending from China to the area east of Japan. The Baiu front may be located at a position where convective clouds are aligned. It does not have a large temperature gradient and does not correspond closely to the upper strong wind axis. In the water vapor imagery, a dark region corresponding to a Pacific high is seen over southern Japan and around the Korean Peninsula across a bright region in a long thin belt form corresponding to the Baiu front. The dark region **N** to the north is a dry area formed by subsidence associated with anticyclonic conditions in the mid-latitudes. The dark region **S** to the south corresponds to the Pacific high.

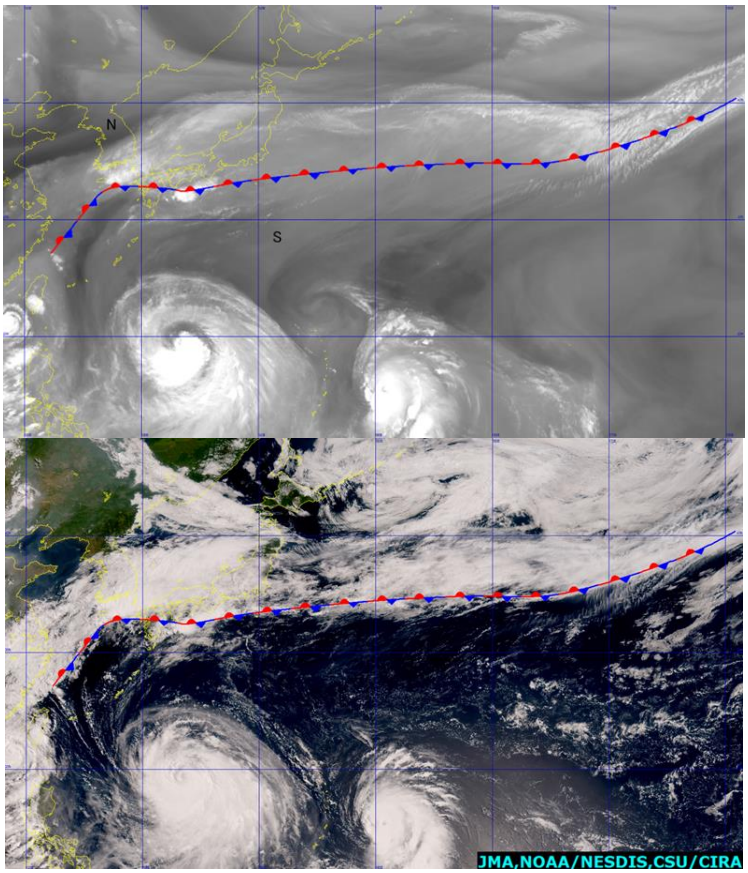

Fig. 5-1-18. Baiu front at 00:00 UTC on 8 July 2015
Top: B10 water vapor image, 300-hPa isohypse; bottom: True Color Reproduction image (see the main text for alphabetical designations)

5.2. Classification of Cyclonic Development Patterns

The Bergen School Cyclone Model proposed by J. Bjerknes and Solberg in the 1920s remains the most common representation of cyclone system lifespans. Based mostly on surface observation data and resulting insights, it comprehensively expresses the concepts of cyclogenesis from frontal waves in the mid-latitudes onward. As is evident from satellite observation of cyclogenesis, the model supports ready recognition of cloud patterns. The cloud model of these types is regarded here as standard.

Observation of cyclone lifespans in satellite imagery also reveals patterns other than the standard type (Fig. 5-2-1). Accordingly, developmental patterns not covered by the Bjerknes model are separately characterized for satellite imagery. Specifically, these are comma-type and instant occlusion-type phenomena occurring poleward from the mid-latitude baroclinic zone. Comma-type cyclones develop until comma-shaped cloud areas come into contact with a mid-latitude frontal zone after descending southward from the polar side of a baroclinic area. In instant occlusions, a rapid shift toward an occlusion pattern is seen as frontal cloud bands merge with such comma-shaped areas. Shapiro and Keyser (1990) presented a developmental model for T-bone-shaped cloud patterns as a type of cyclone developing in baroclinic zones. Here, the structure around the cyclonic center is governed by the detachment mechanisms of fronts and warm nuclear isolation, representing cloud areas different from those of the Bjerknes model.

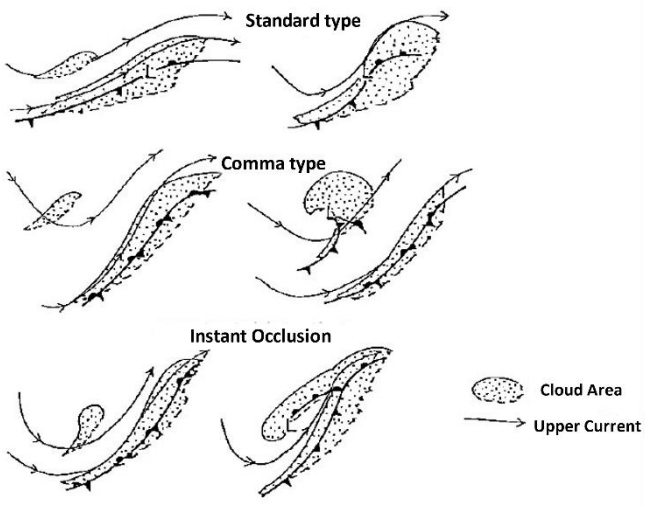

Fig. 5-2-1. Standard, comma and instant occlusion models

This chapter outlines the characteristics of each cloud pattern in the context of synoptic-scale cyclonic development. Various forms of cyclogenesis recognizable in satellite imagery outside the scope of the Bjerknes model are also presented, as these models were developed in relation to Western areas and cyclonic behavior around Japan may differ due to greater sub-tropical influence in the relevant lower latitudes.

The terms “development stage” and “mature stage” here are judged from satellite imagery, and may not match the cyclogenesis stages seen in weather charts. The mature stage in satellite imagery is considered to be reached slightly earlier than the lowest cyclonic pressure period. In frontal drawing too, analysis is focused on satellite imagery, and may not necessarily match that derived from weather charts.

5.2.1. Standard-type Development

As reported by Yamada and Suzuki (1994), the standard type represents approximately a third of cyclones rapidly developing over the sea east of Japan in winter, typically taking three days after emergence to reach maturity. In satellite imagery, the characteristics seen in the formative and development stages are cloud area formation and northward ascent associated with warm advection at the front of the cyclone, with cloud areas dissipating and descending southward in association with dry cold inflow at the rear of the cyclone. These characteristics represent the development of baroclinic instability via frontal waves, as readily highlighted by the Bjerknes model.

Okabayashi (1982) proposed a cyclogenesis cloud model based on the Bjerknes model (Fig. 5-2-2) as represented in the standard-type example shown below. Temporal changes in cyclonic central pressure here are illustrated in Fig. 5-2-3. The formative and development stages correspond to the development stage in the example.

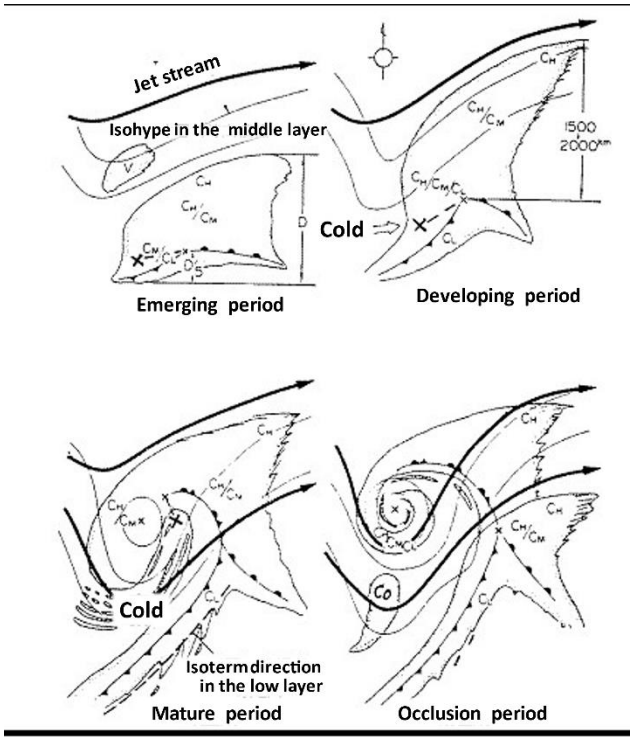

Fig. 5-2-2. Cyclone model (Okabayashi, 1982)

X represents the cyclonic center, **x-x** is the area encompassing the center, and **CH**, **CM** and **CL** represent upper, middle and lower clouds, respectively.

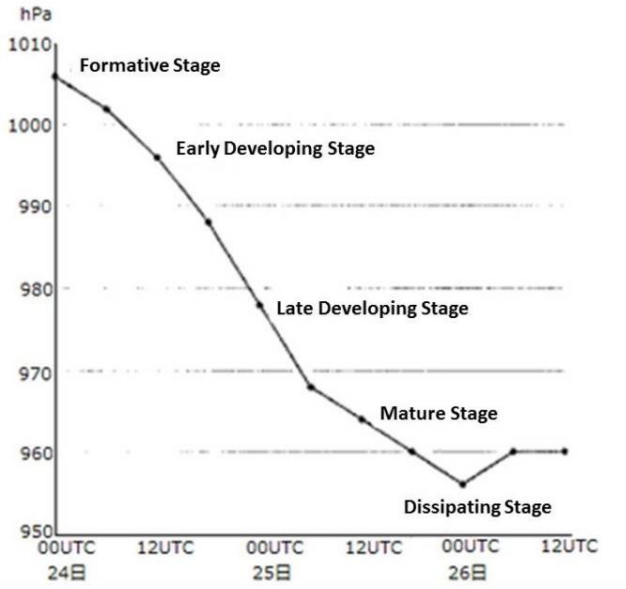

Fig. 5-2-3. Temporal changes in cyclonic central pressure

1. Formative Stage (Fig. 5-2-4)

In the early stages of baroclinic-zone disturbances, a cloud pattern with an S-shaped edge (known as a cloud leaf or baroclinic leaf form) appears, as sometimes observed between the East China Sea and the Sea of Japan. This morphology is associated with warm conveyor belt (WCB) wet currents, indicating a strengthening of warm advection.

Cyclone centers in the formative stage are hard to identify from cloud patterns, tending to be positioned near the center or around the southern edge of the cloud area. In this example, the cyclone and the front are considered to be in this stage. In the Okabayashi model, the northern edge of the cloud area and the jet stream appear separate but generally in proximity. The jet stream also corresponds to the northern edge of the cloud leaf, based on the analysis position of the boundary and the northern edge of the cloud leaf as clearly seen in the water vapor image.

In the Okabayashi-model formative stage, the area V comprising mostly upper cloud appears to head northwestward toward a cyclonic cloud area. Although not seen here, it should be noted that the cloud area often corresponds to an upper trough, potentially reaching the cyclonic cloud area and exacerbating development.

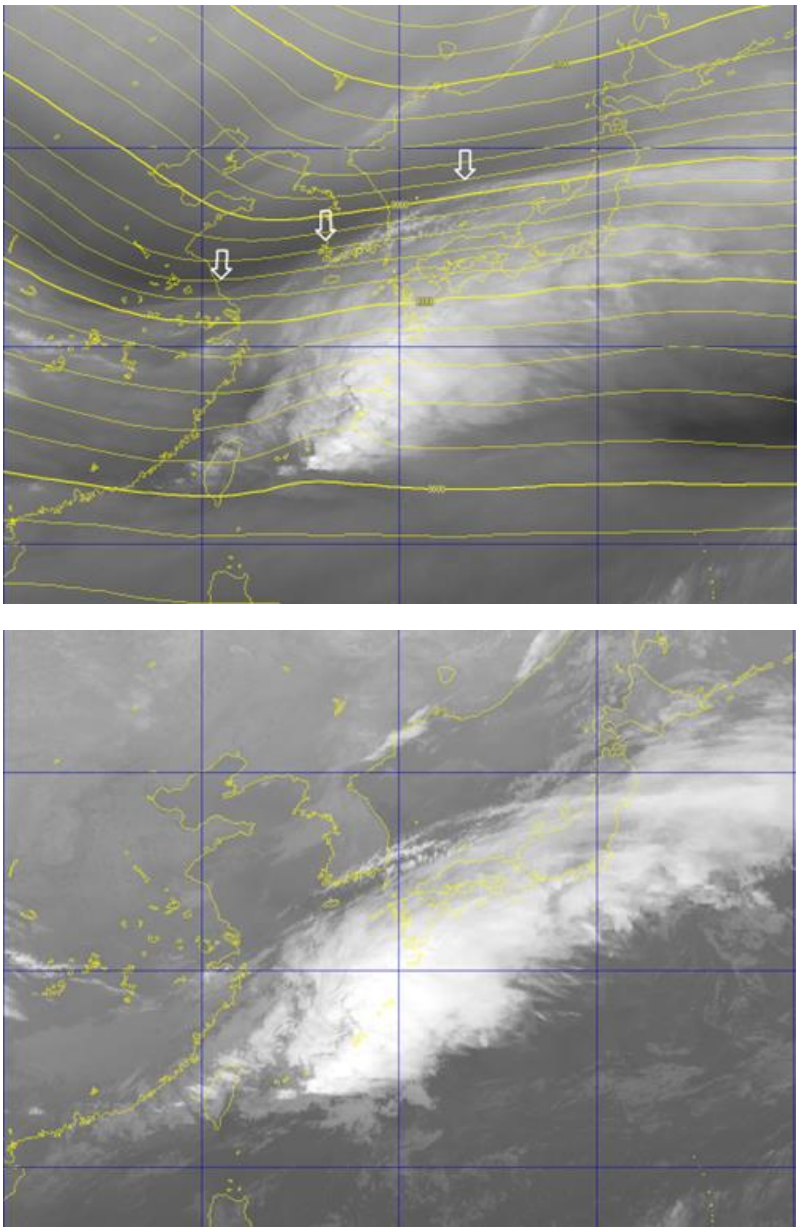

Fig. 5-2-4. Standard type, formative stage, at 18:00 UTC on 13 March 2016
Top: B10 water vapor image with 300-hPa isohypse and arrows marking the boundary; bottom: B13 infrared image

2. Early Development Stage (Fig. 5-2-5)

Bulge patterns in the early development stage with increased anticyclonic curvature at the northern edge of a cloud area expanding northward from a cloud leaf indicate the presence of warm air ascending northward in association with WCB conditions or ascending currents intensifying at the front of a trough. This is a characteristic of the development stage in baroclinic disturbances. The boundary in water vapor imagery corresponding to the upper strong wind axis reveals trough deepening farther southward after formation.

Cyclone centers can often be identified near the start point at the western edge of a bulge as it shifts westward from its center in the formative stage, while identification from cloud

patterns is difficult. Similarly, warm and cold fronts in the formative stage are determinable southward of lower clouds. This stage corresponds to the intermediate state between the formative and the development stages in the Okabayashi model.

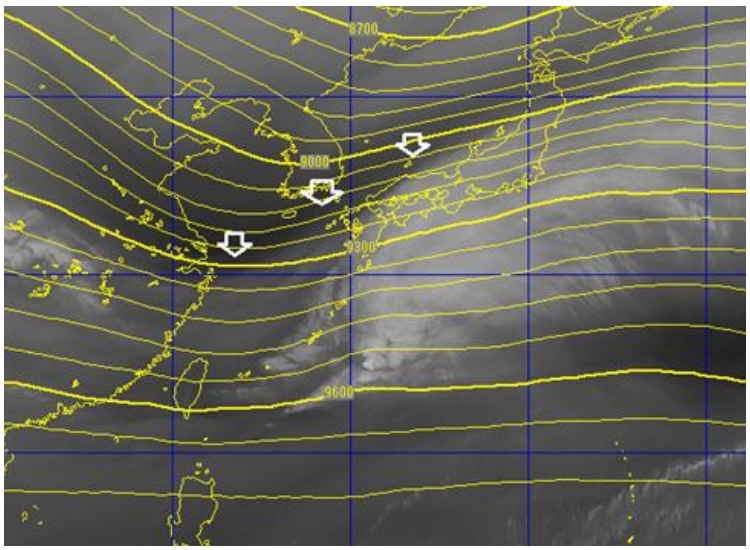

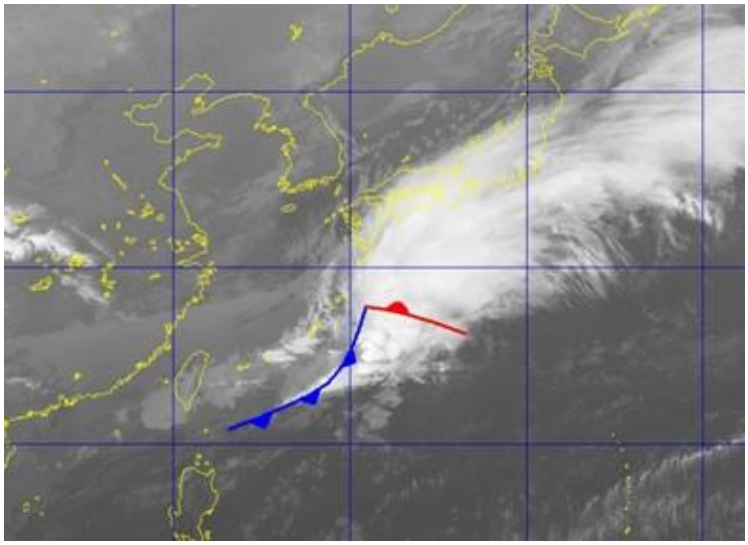

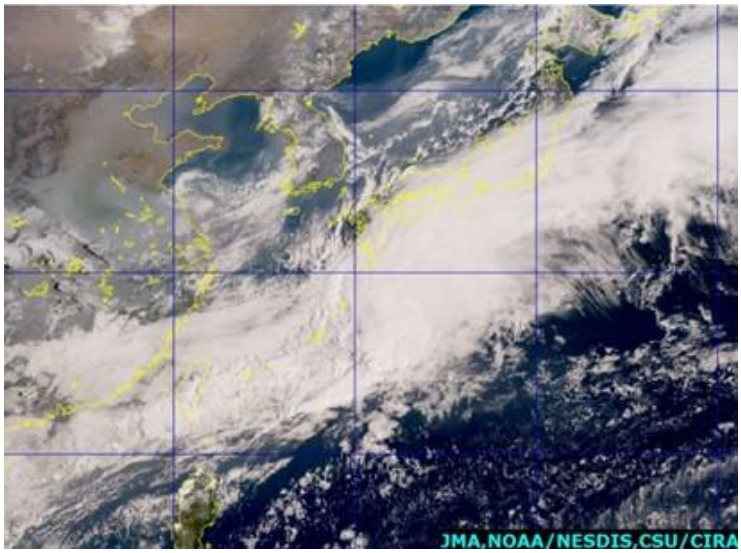

Fig. 5-2-5. Standard type in the early development stage at 00:00 UTC on 14 March 2016
Top: B10 water vapor image with 300-hPa isohypse and arrows marking the boundary;
middle: B13 infrared image: bottom: True Color Reproduction image

3. Late Development Stage (Fig. 5-2-6)

This is equivalent to the development stage in the Okabayashi model. Bulges are clearer, with streaky cloud at the rear of the cyclone indicating an inflow of cold air that forms a hook pattern. The cloud area has a meridional strike extending farther than in the early development stage. The meridional elongation of this area corresponds to the strengthened effects of cold advection at the rear of the cyclone and warm advection at its front.

The Okabayashi model poses the potential for association between the cyclonic center and the center of the cloud area at this stage. However, in this example, the center of the cyclone is farther west in the cloud area than in the early development stage, and a hook is observed at the western edge of the cloud. A cloud band is also prominent in correspondence to the cold front in association with cold inflow.

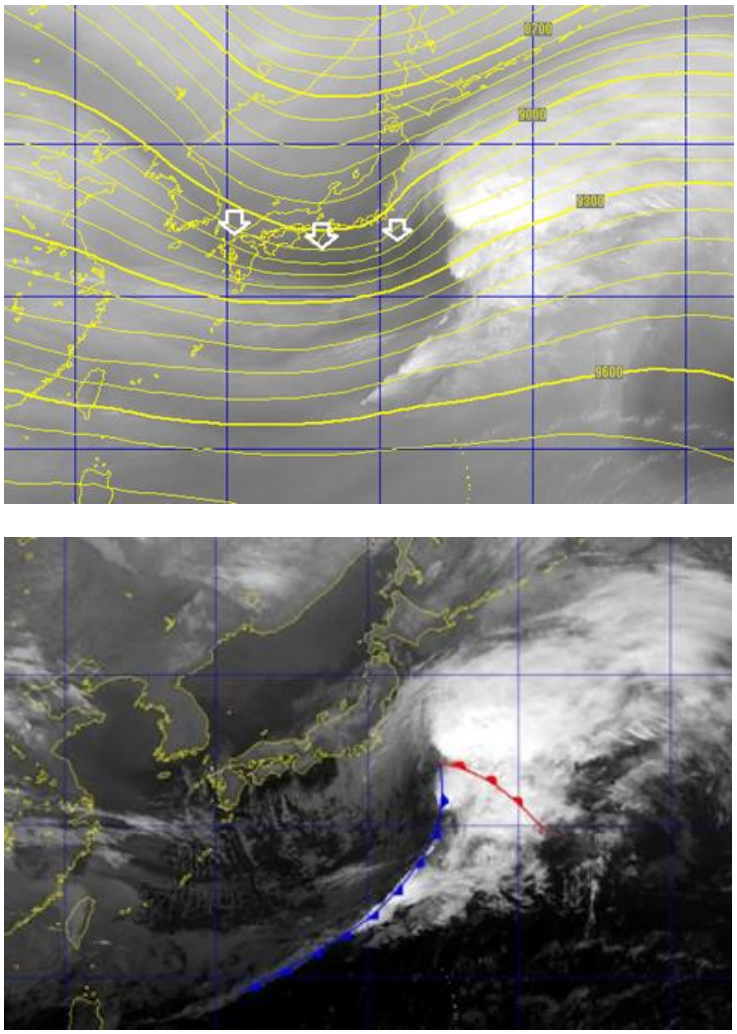

Fig. 5-2-6. Standard type, late development stage, at 18:00 UTC on 14 March 2016
Top: B10 water vapor image with 300-hPa isohypse and arrows marking the boundary;

bottom: B13 infrared image

4. Mature Stage (Fig. 5-2-7)

This is equivalent to the mature stage in the Okabayashi model, with a comma-type cloud pattern forming as a dry-air slot intrudes into the vicinity of the center. In satellite imagery, the cloud edge is distinct with a high top, and is determinable as the most developed stage. Central cyclonic pressure continues to fall, although the minimum pressure is not yet reached. Streaky cloud at the rear of the cyclone indicates intense cold-air intrusion.

The cyclone center can be determined from a lower vortex near a dry slot, with the occluded front at the western edge of a cloud area in contact with the boundary of this slot. In water vapor imagery, this is seen as a progressive darkening of a region downstream of the boundary, implying intrusion of dry air from the upper layer to the rear of the developed cyclone. Here, the occluded front is not above the cloud top on the western edge, but is farther rearward in the lower cloud area. Such patterns may arise when a dry slot surpasses a surface occluded front.

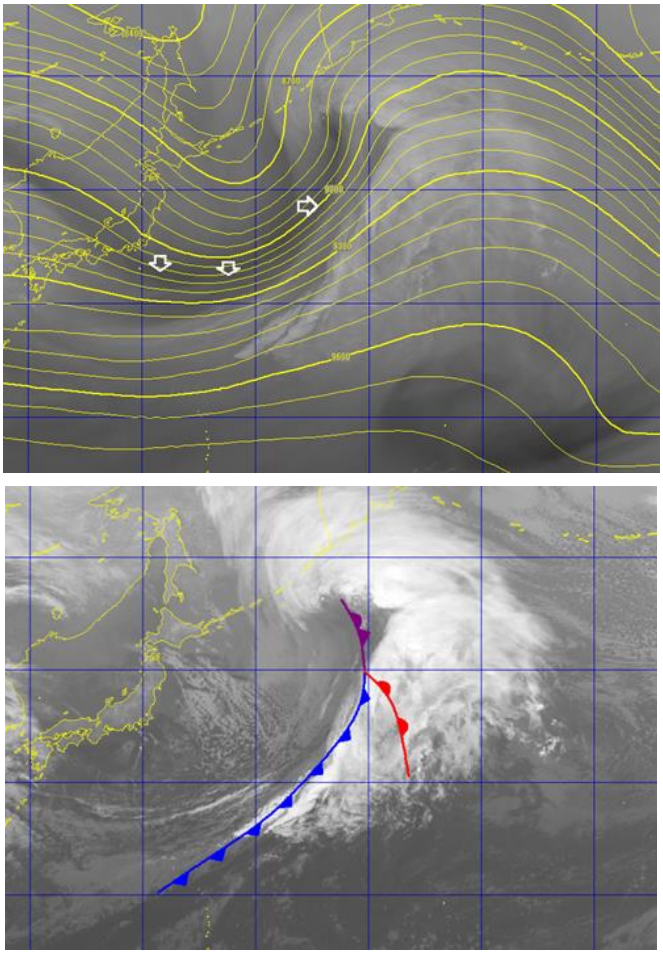

Fig. 5-2-7. Standard type, mature stage, at 12:00 UTC on 15 March 2016
Top: B10 water vapor image with 300-hPa isohypse and arrows marking the boundary;
bottom: B13 infrared image

5. Dissipation Stage (Fig. 5-2-8)

This corresponds to the occlusion stage in the Okazaki model. At the cyclonic center, convective activity decreases with lowering of the cloud top, and a lower vortex emerges. In response to cold air associated with a short-wave trough blowing from the rear of the cyclone, enhanced Cu (**E**) is seen (equivalent to the Co cloud area in the Okazaki model), and may further develop into comma cloud forms. A higher cloud-top region with active convection is seen in the vicinity of the occlusion point. The dry slot, which surpasses the surface occluded point at the mature stage, moves parallel again to this front with entwined motion around the cyclonic center.

The cloud top is lowered overall, featuring a looser edge with lower clarity as dissipation progresses. Characteristics seen in the dissipation stage include a lowering of the cloud top, particularly around the cyclonic center, and termination of darkening at the dry slot along with enhancement of the bright region. The lowest period of cyclonic central pressure in the cyclonic lifecycle is often observed after the beginning of dissipation recognizable in satellite imagery.

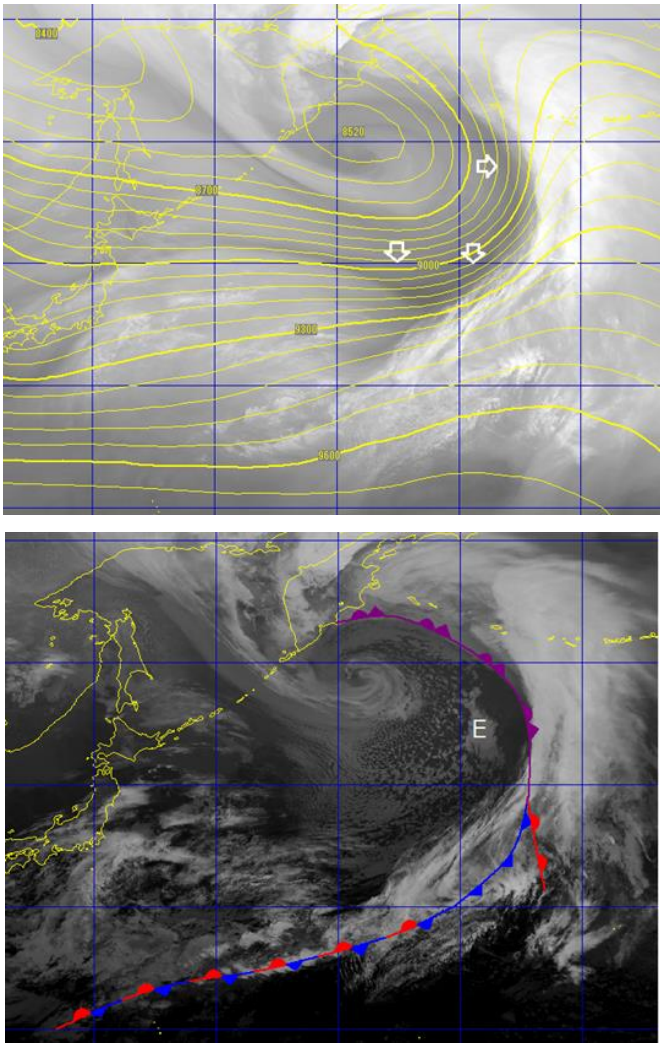

Fig. 5-2-8. Standard type, mature stage, at 12:00 UTC on 16 March 2016
Top: B10 water vapor image with 300-hPa isohypse and arrows marking the boundary;

bottom: B13 infrared image

5.2.2. Comma-type Development

Comma clouds form on the polar side of mid-latitude baroclinic zones, often during cold periods. Cyclonic conditions corresponding to comma clouds are known as polar lows, which differ from the standard type in development. Comma-cloud formation requires an updraft from positive vorticity advection in the middle layer, along with sensible and latent heat from a warm sea surface. Such clouds may emerge on a small scale in regions with weak baroclinicity, but baroclinic instability is also required for synoptic-scale cyclonic development as described below.

Reed and Blier (1986; Fig. 5-2-9) presented a comma-type cloud development model in which convective clouds emerge near positive vorticity advection during the formative stage but no structural organization is yet apparent. In the development stage, comma-type clouds form in cyclonic conditions observable at the top of the comma. Warm advection is initiated in front of the cloud area, and cold advection intensifies at its rear. During the mature stage, clouds move ahead of a long wave trough, and the tail segment acquires cold-front characteristics.

Comma clouds developing over seas east of Japan and elsewhere emerge in cold air away from major baroclinic zones. At the beginning of the formative stage, the cloud area comprises an open cell corresponding to a short-wave trough or enhanced Cu. This indicates the key roles of sensible and latent heat from the sea surface in development. The cloud area takes on comma-type characteristics as it moves to the front of the main trough.

Over the warm Sea of Japan, comma clouds tend to develop rapidly when dry air moves in from the continental area, where formation is less likely even in positive vorticity advection fields. Suzuki and Yamada (1994) reported that comma clouds take around 12 hours less to reach maturity from the formative stage than the standard type.

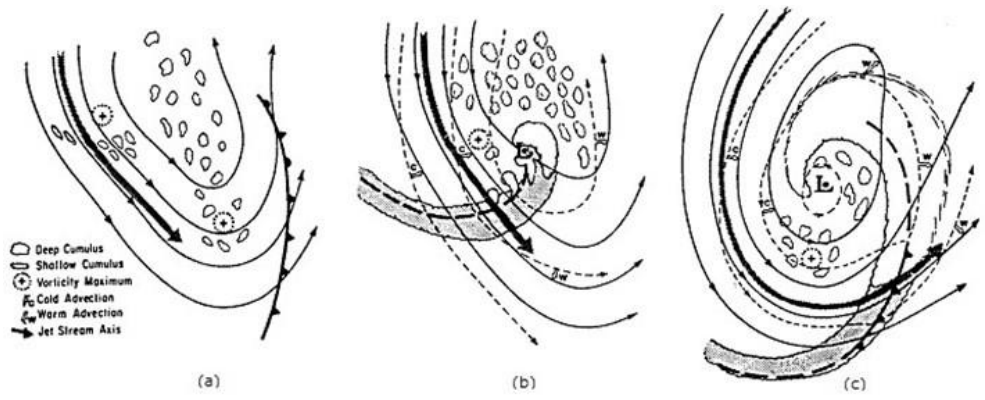

Fig. 5-2-9. Comma-cloud model (Reed and Blier, 1986)
(a) Formative stage (b) Development stage (C) Mature stage
(solid lines: 500 hPa isohypse; dashed lines: isobars above ground)

(1) Sea-area Comma Clouds

1. Formative Stage (Fig. 5-2-10)

The cloud area (B) over the Bering Sea in the figure corresponds to a well-developed cyclone, behind which cell-form convective clouds associated with cold-air advection are observed. Over the Sea of Okhotsk and the sea southeast of Kamchatka, active cell-form convective clouds are seen with an open structure in association with the cold air. The solid area **A** with upper clouds also begins to develop, representing the emergence of an as-yet unrecognizable comma cloud formation.

This area forms in association with maximum positive vorticity advection (PVAmax) in front of a short-wave trough intruding at the rear of a cold low east of Kamchatka. Cloud density at this stage is uneven, with no anticyclonic curvature at the cloud edge. The area **A** does not appear organized at this pre-cyclonic stage.

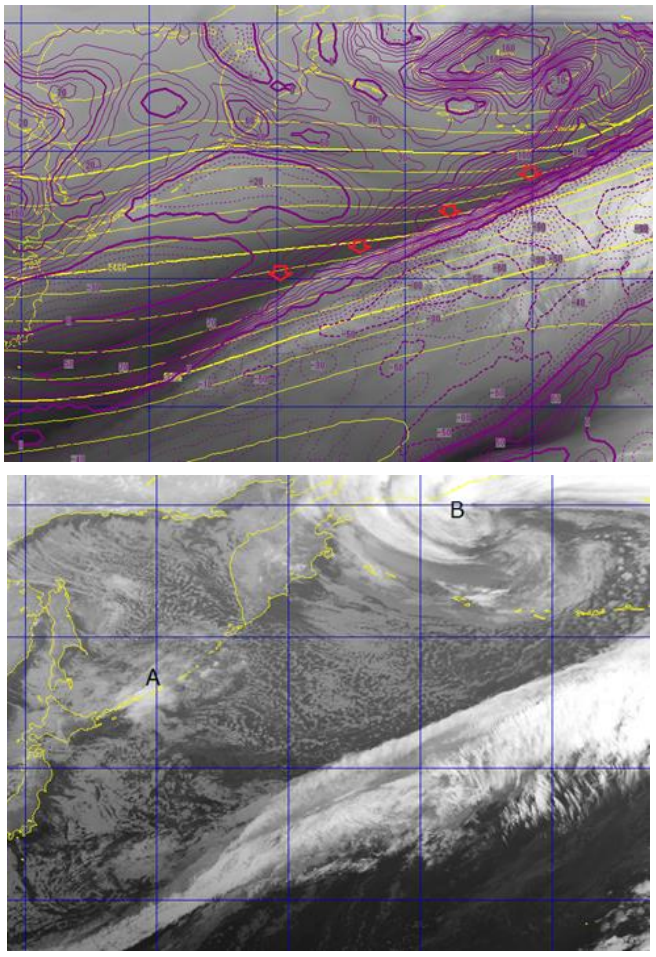

Fig. 5-2-10. Comma cloud over the sea, formative stage, at 12:00 UTC on 18 December 2015. Top: B10 water vapor image with 500-hPa isohypse and vorticity (solid line: positive; dashed line: negative); bottom: B13 infrared image with arrows marking the boundary

2. Early Development Stage (Fig. 5-2-11)

The cloud area **A** here increases both in density and top height. At its northern edge, upper

cloud shows comma-shaped anticyclonic curvature. The enhanced Cu (**E**) to the west of **A** indicates the presence of a cold-air core behind the cloud area (i.e., in front of a trough associated with this air). There are fewer cell-form clouds at the front of cloud area **G**, indicating cold-air weakening. The weaker cold at the front of this area (which may alternatively be warm advection) and the presence of intense cold air at the rear are as per the Reed and Blier model.

Based on those observations, cloud area **A** is considered to have assumed a baroclinic development process. At this stage, the area began to form a comma-type shape with cyclonic conditions at its southern edge.

PVAmax intensifies after the formative stage. The comma cloud area **A** to the north of the boundary corresponds to the jet stream, manifesting at the polar side of the mid-latitude frontal zone.

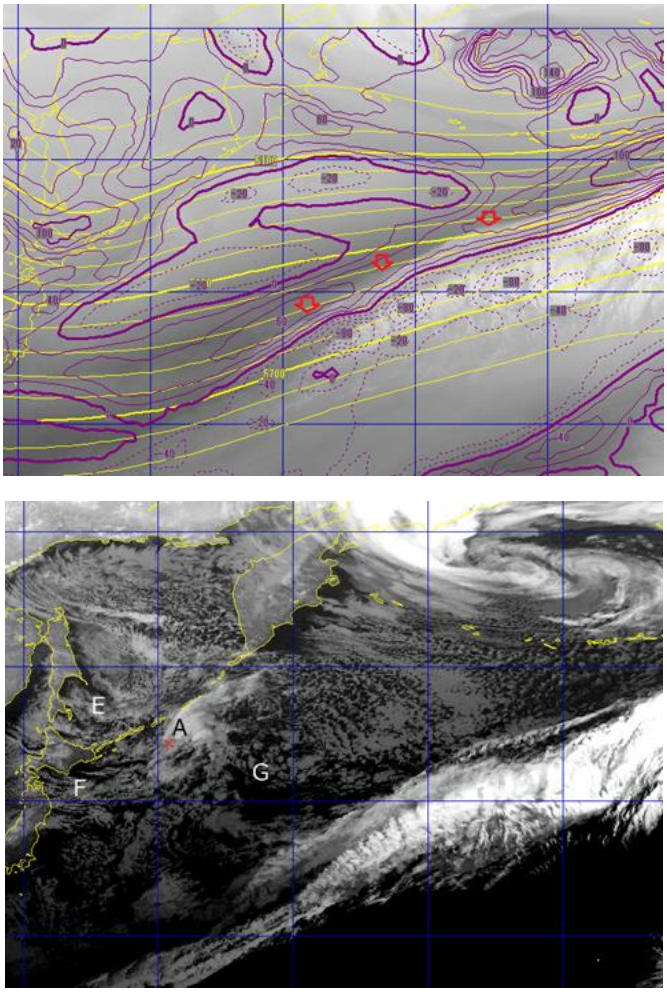

Fig. 5-2-11. Comma clouds over the sea, early development stage, at 18:00 UTC on 18 December 2015. Top: B10 water vapor image with 500-hPa isohypse and vorticity (solid line: positive; dashed line: negative); bottom: B13 infrared image

3. Late Development Stage (Fig. 5-2-12)

Anticyclonic curvature in this stage increases at the northern edge of the cloud area, creating

a clearer overall comma shape with a head comprising tall clouds featuring a near-uniform top height, and a tail comprising active convective clouds. The comma shape represents an organized disturbance with PVA max values retained. The cloud line of the comma tail becomes distinct.

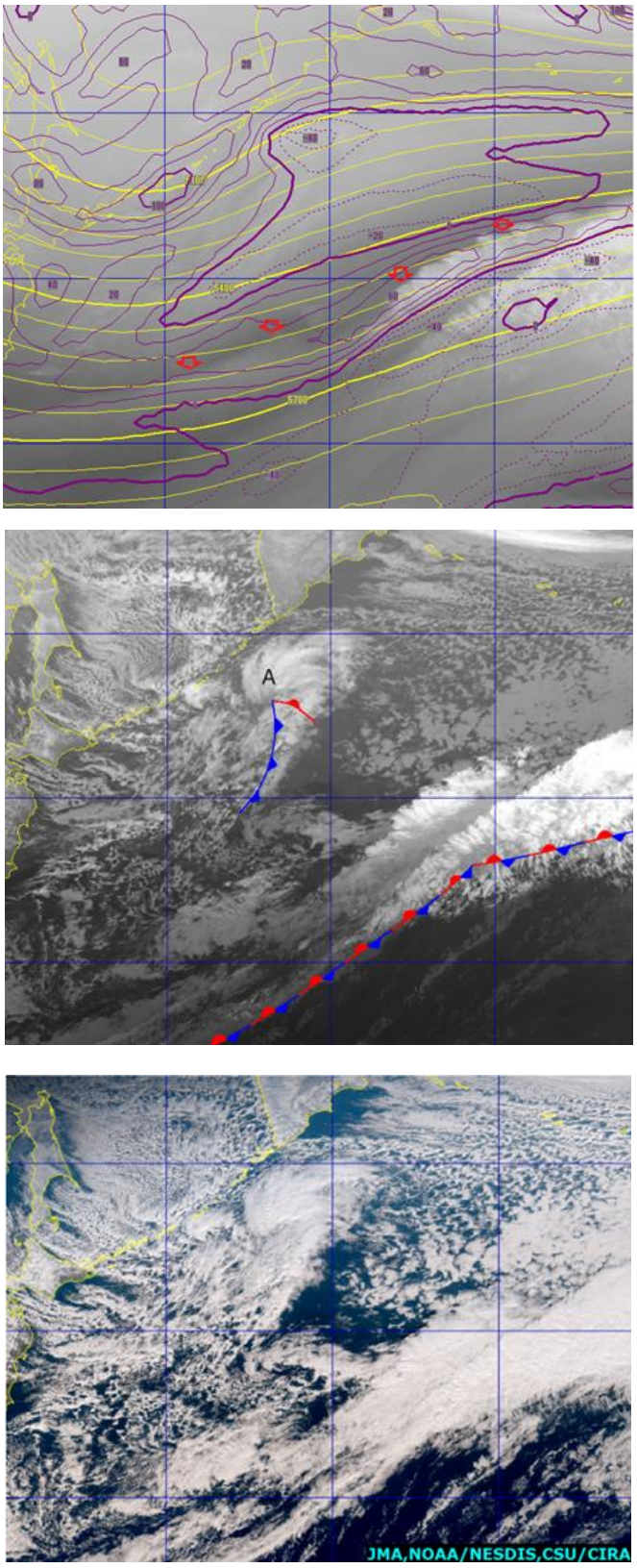

Fig. 5-2-12. Comma clouds developing over the sea, late development stage, at 00:00 UTC on 19 December 2015. Top: B10 water vapor image with 500 hPa isohypse and vorticity (solid line: positive; dashed line: negative) and arrows marking the boundary. Middle: B13 infrared image; bottom: True Color Reproduction image

4. Mature Stage (Fig. 5-2-13)

In the presence of a clear dry slot, the mature stage is reached here with the same pattern as the standard type. The cloud area measures 1,000 – 1,500 km, which is smaller than the standard type. In the figure, comma cloud development is seen in association with trough deepening around a cold low near the Kamchatka Peninsula. In contrast to the standard type, the boundary corresponding to the jet stream is still positioned south of the comma cloud. Comma-type development occurs rapidly between the initial identification of low ground pressure and maturity. It is recognized in satellite imagery as a solid cloud area before assuming cyclonic characterization.

Here, a cloud band corresponding to a stationary front is seen at 40° north latitude. Although the comma cloud and the cloud band are in close proximity, they develop individually and separately. When these areas reorganize a single mass via reciprocal influence, they are seen as an instant occlusion-type development.

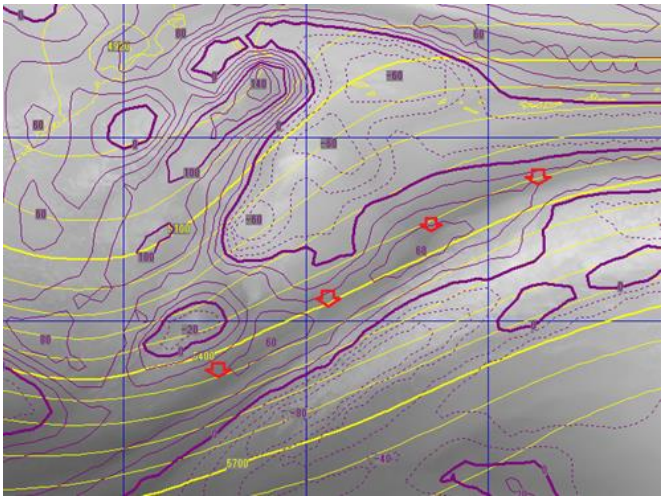

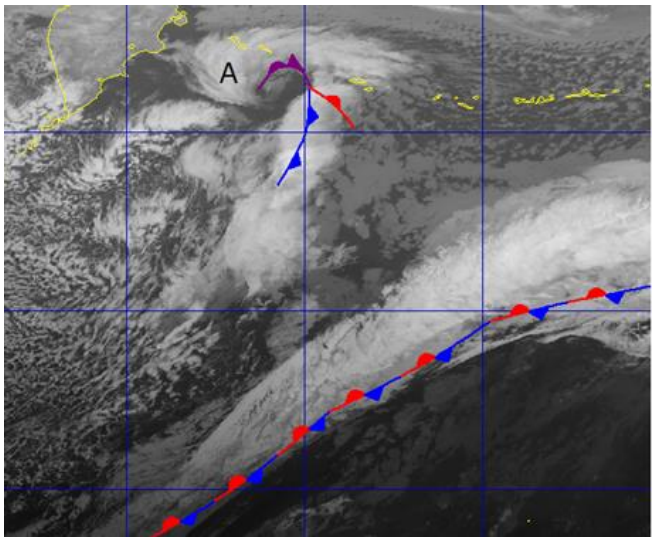

Fig. 5-2-13. Comma cloud development over the sea, mature stage, at 18:00 UTC on 19 December 2015. Top: B10 water vapor image with 500-hPa isohypse and vorticity (solid line: positive; dashed line: negative) and arrows marking the boundary.
Bottom: B13 infrared image

(2) Development of Comma Clouds Around Japan

1. Formative Stage (Fig. 5-2-14)

When the Ci area **A** approaches the Sea of Japan from the continent, the cloud area **B** containing convective clouds here rapidly develops into a Cb area over the western Sea of Japan. This Ci corresponds to an upper trough, and its movement can be tracked back to the continent. Convective clouds emerge rapidly, often taking 3 – 6 hours to develop into an organized area from a cloudless state around Japan (here, Cu moves eastward and convective cloud containing Cb (**B**) subsequently emerges 3 – 4 hours later around 15:00 UTC). The cloud area **B** is in front of a trough at 500 hPa, corresponding to an updraft based on PVAmax. As the convective cloud mass grows, it takes on an organized structure. At this point, a cyclone is identifiable in the vicinity of **x**.

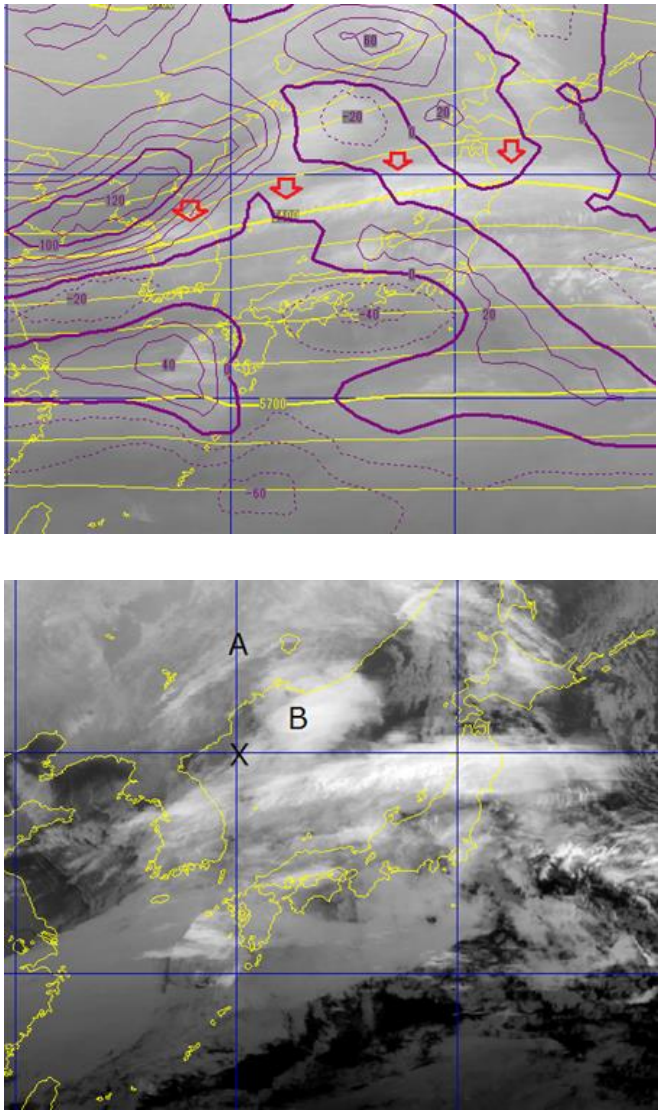

Fig. 5-2-14. Comma cloud development near Japan, formative stage, at 18:00 UTC on 15 December 2014. Top: B10 water vapor image with 500-hPa isohypse and vorticity (solid line: positive; dashed line: negative) and arrows marking the boundary.
Bottom: B13 infrared image

2. Development Stage (Fig. 5-2-15)

The cloud area here forms a comma shape with a distinct notch, an elevated top height and increased convective activity at its tail. A streaky cloud line emerges at its rear due to cold-air inflow, and the mass advances in front of the trough at 500 hPa maintaining corresponding to PVAmax.

As previously described, comma clouds near Japan characteristically develop more quickly after emergence than those developing over seas east of the country. This is attributed to cold air from the continent causing rapid instability over the warm Sea of Japan. At the comma tail, convective clouds rapidly develop to create a clear cold-front structure, raising the likelihood of phenomena such as rapid changes in wind direction, gusting winds and intense

rainfall. Accordingly, satellite monitoring of these phenomena is essential.

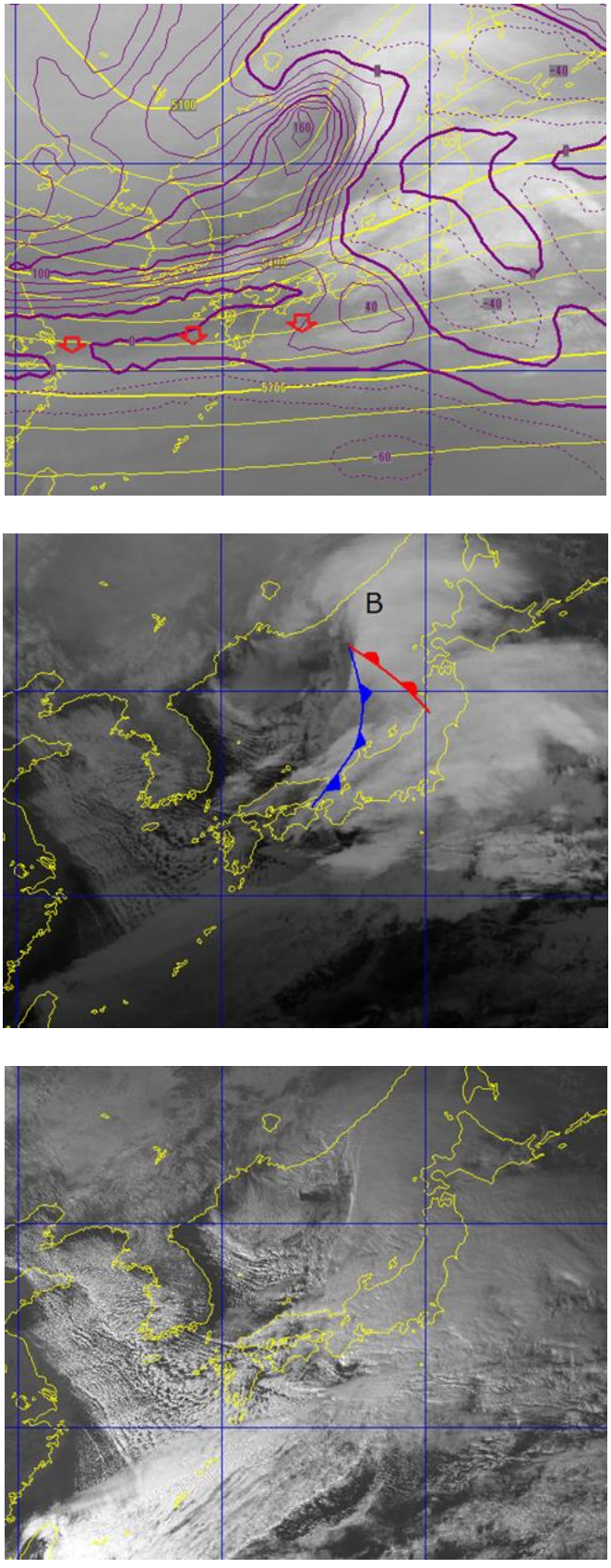

Fig. 5-2-15. Comma-cloud development near Japan, development stage, at 06:00 UTC on 16 December 2014. Top: B10 water vapor image with 500-hPa isohypse and vorticity (solid line:

positive; dashed line: negative) and arrows marking the boundary; middle: B13 infrared image; bottom: B03 visible image

3. Mature Stage (Fig. 5-2-16)

A dry slot is seen here over the sea west of Hokkaido. The cloud top is raised in the area corresponding to the comma head, indicating maturation. Comma clouds rapidly developing near Japan bring intense cold air along with streaky convective cloud at the rear of the cyclone, indicating further development. Subsequent development follows the pattern of comma clouds observed over the sea east of Japan.

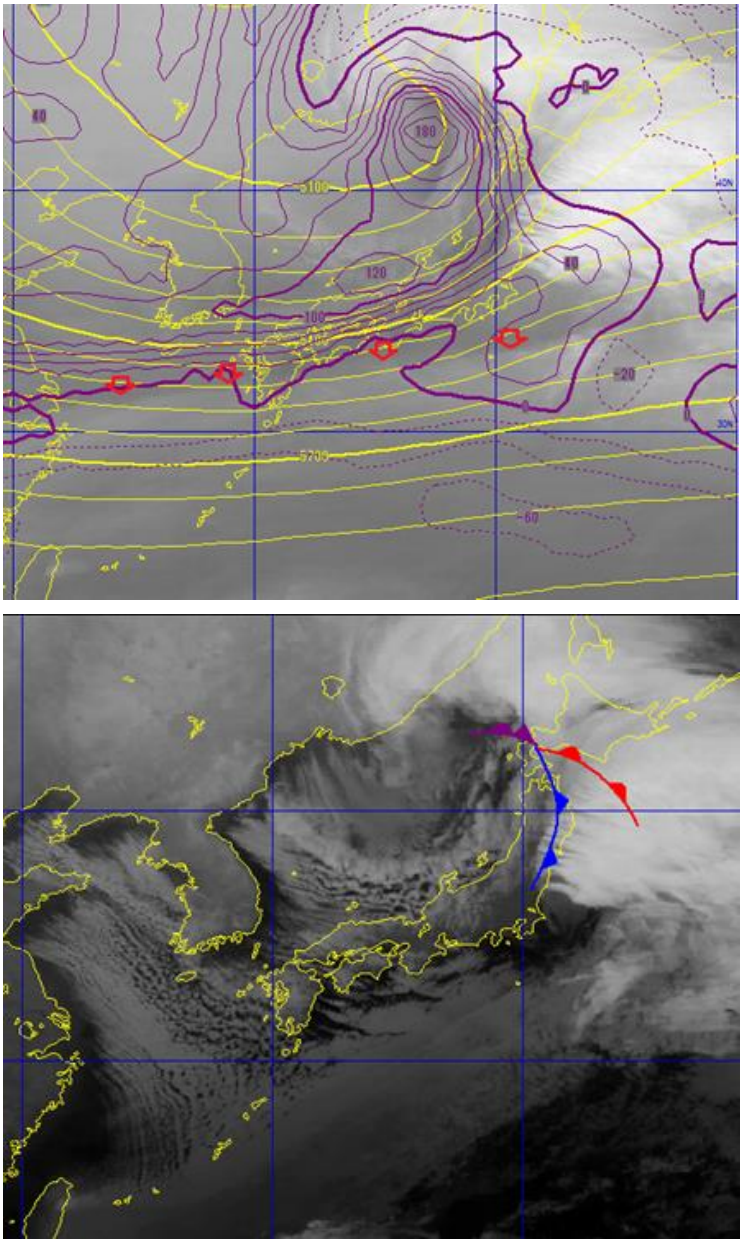

Fig. 5-2-16. Comma clouds near Japan, mature stage, at 12:00 UTC on 16 December 2014.
Top: B10 water vapor image with 500-hPa isohypse and vorticity (solid line: positive; dashed line: negative) and arrows marking the boundary.
Bottom: B13 infrared image

5.2.3. Instant Occlusion-type Development

The instant-occlusion cyclone development process observed in satellite imagery indicates cloud patterns in the occluded stage resulting from comma clouds merging with a frontal cloud band. In contrast to the standard type, occluded-cloud patterns form instantly with no development stage. Figure 5-2-17 (Kitabatake, 1997) summarizes the two models proposed by Browning and Hills (1985; the BH model) and McGinnigle, Young and Bader (1988; the MYB model). The key feature of the BH model is a polar-trough conveyor belt (PTCB), which is a lower-level airflow moving poleward from a frontal cloud band. The baroclinicity of comma clouds is not seen as critical in this situation. In the MYB model, warm advection along comma clouds and updrafts associated with positive vorticity advection have critical roles, and an occlusion pattern is reached via the formation of new clouds between comma clouds and the frontal cloud band.

The MYB and BH models are more applicable to cases with and without cyclone development, respectively.

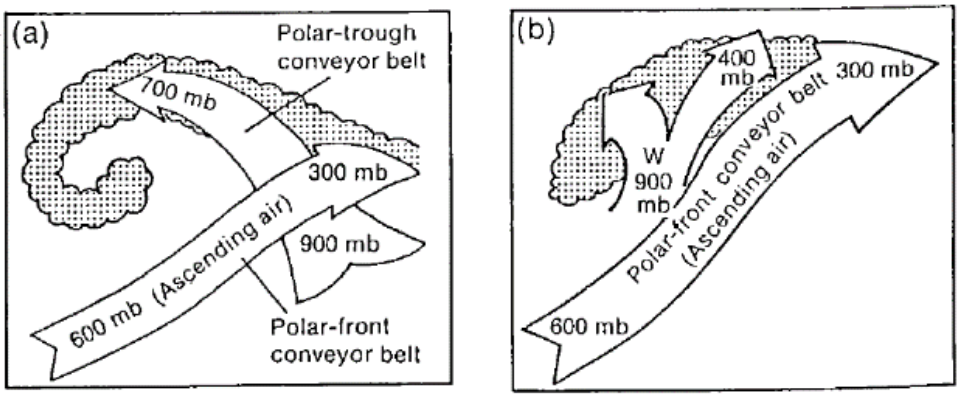

Fig. 5-2-17. Instant occlusion (Kitabatake, 1997)
(a): BH model; (b): MYB model

(1) No Further Cyclone Development (BH model)

1. Initial Stage (Fig. 5-2-18)

A cyclone corresponding to the comma-type cloud area **A** is seen east of Japan here, progressing east-northeastward. An area of upper- and middle-layer clouds **D** is observed in association with the front south of around 30° north latitude, with a southwest-northeast strike direction. The bulge observed takes on an anticyclonic curvature to the north of the cloud band upon approach.

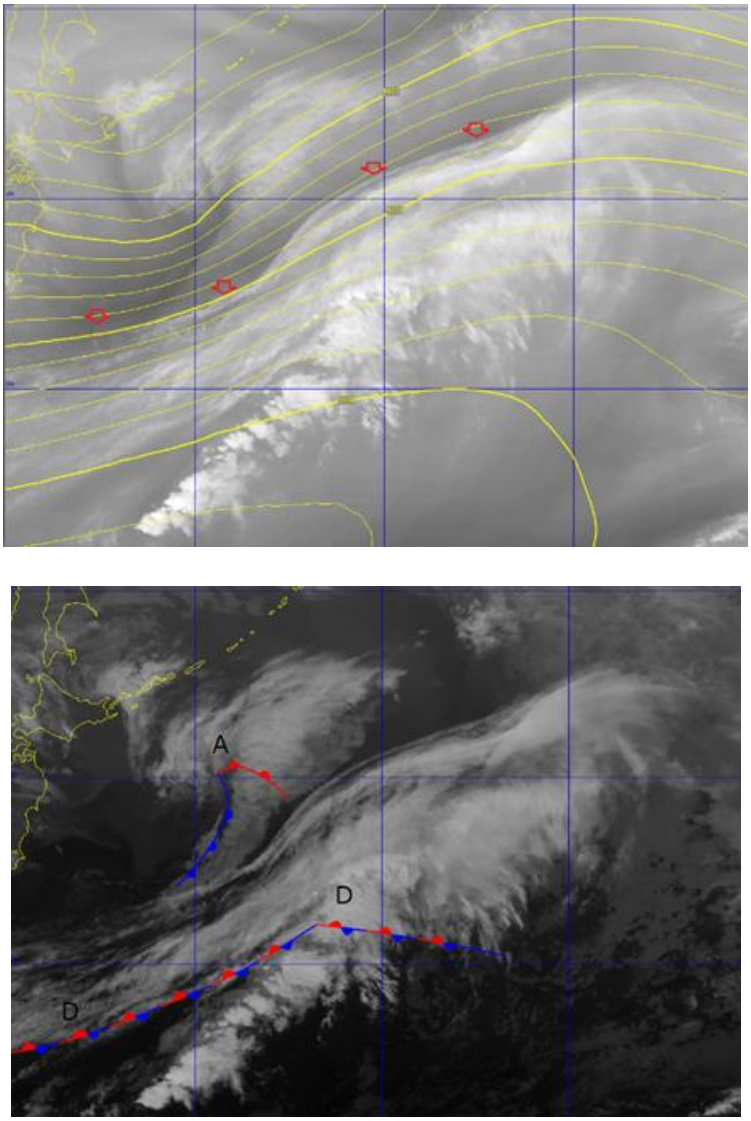

Fig. 5-2-18. Instant occlusion with no development (BH model), initial stage, at 18:00 UTC on 25 April 2011. Top: B10 water vapor image with 300-hPa isohypse and arrows marking the boundary; bottom: B13 infrared image

2. Occlusion Commencement Stage (Fig. 5-2-19)

The distance between the comma cloud **A** and the cloud band **D** here is reduced. Characteristics include a distinctive long tail with a raised top at the head of the comma cloud, increased density at the part of the band in contact with this cloud, and a heightened top in the cloud band. These characteristics represent synergetic effects between the comma and band clouds. However, the gap between the cloud band and the comma tail suggests the PTCB is insufficiently formed, and no occlusion pattern has yet developed.

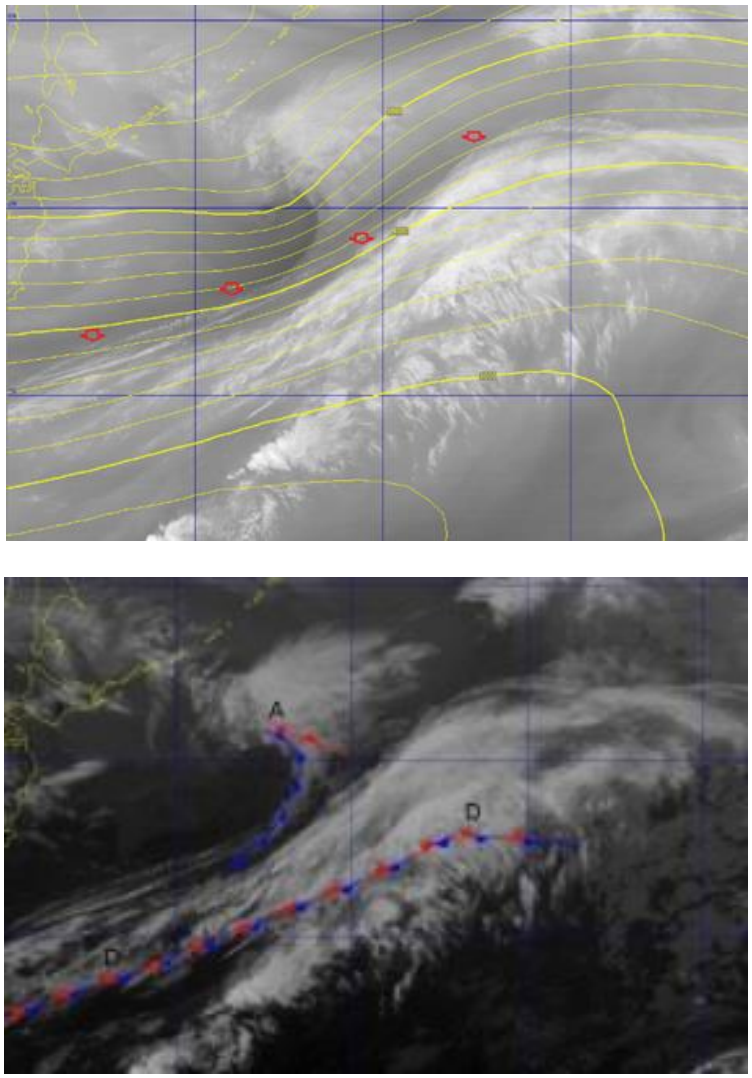

Fig. 5-2-19. Instant occlusion with no development (BH model), occlusion commencing, at 00:00 UTC on 26 April 2011. Top: B10 water vapor image with 300-hPa isohypse and arrows marking the boundary; bottom: B13 infrared image

3. Occlusion Completion Stage (Fig. 5-2-20)

The top height here is raised at the tail of the comma cloud **A** in contact with the cloud band **D**, forming an organized band with PTCB formation. In the cloud band corresponding to the frontal zone, the top rises rapidly at the part in contact with the comma cloud tail, with increased anticyclonic curvature at the northern edge. Completion of the instant occlusion is seen at this stage in satellite imagery.

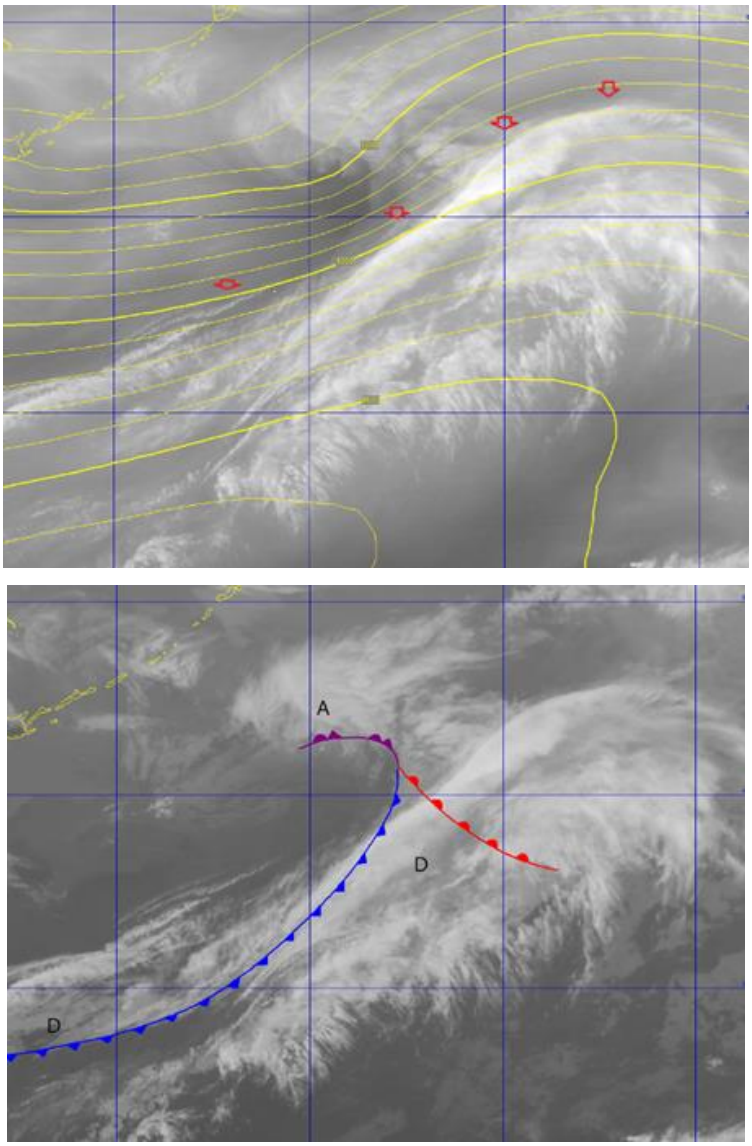

Fig. 5-2-20. Instant occlusion with no development (BH model), occlusion completed, at 06:00 UTC on 26 April 2011. Top: B10 water vapor image with 300-hPa isohypse and arrows marking the boundary; bottom: B13 infrared image

4. Dissipation Stage (Fig. 5-2-21)

The top height decreases here in the cloud band **D** corresponding to the occluded front, becoming obscure with a dissipating tendency. The cyclonic central pressure remains almost the same after the occlusion, with no further development. In the BH model, no further post-occlusion development is seen, and ready movement into the dissipation stage is observed in contrast to the output of the MYB model described below.

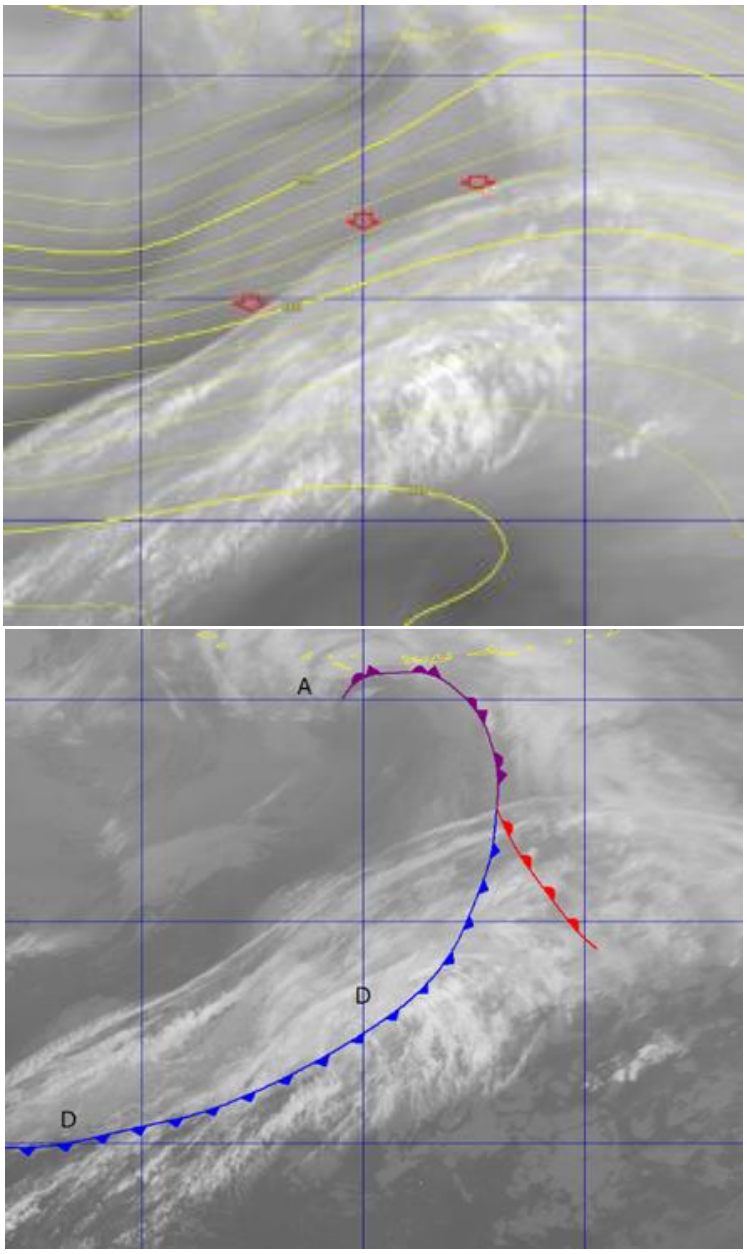

Fig. 5-2-21. Instant occlusion with no development (BH model), dissipation stage, at 00:00 UTC on 27 April 2011. Top: B10 water vapor image with 300-hPa isohypse and arrows marking the boundary; bottom: B3 infrared imagey

(2) With Cyclone Development (MYB model)

1. Initial Stage (Fig. 5-2-22)

The frontal cloud band **B-B** here extends east-northeastward over the sea south of Japan. The comma cloud formation with the obscure tail **N** is seen east of Hokkaido, advancing east-northeastward with an increasing top height. Off the Sanriku shore between the frontal cloud band and the comma cloud, the high-top cloud area **M** emerges, connecting the comma cloud in the north and the frontal cloud band in the south. A cyclone (marked with **x**) corresponding to the comma cloud and a front corresponding to the cloud band can be seen. At 850 and 700 hPa, southwestern wind is prominent with intensified warm advection off the Sanriku coast

(not shown), corresponding to the development of the cloud **M** to the warm side of the comma cloud. These are typical characteristics of the MYB model.

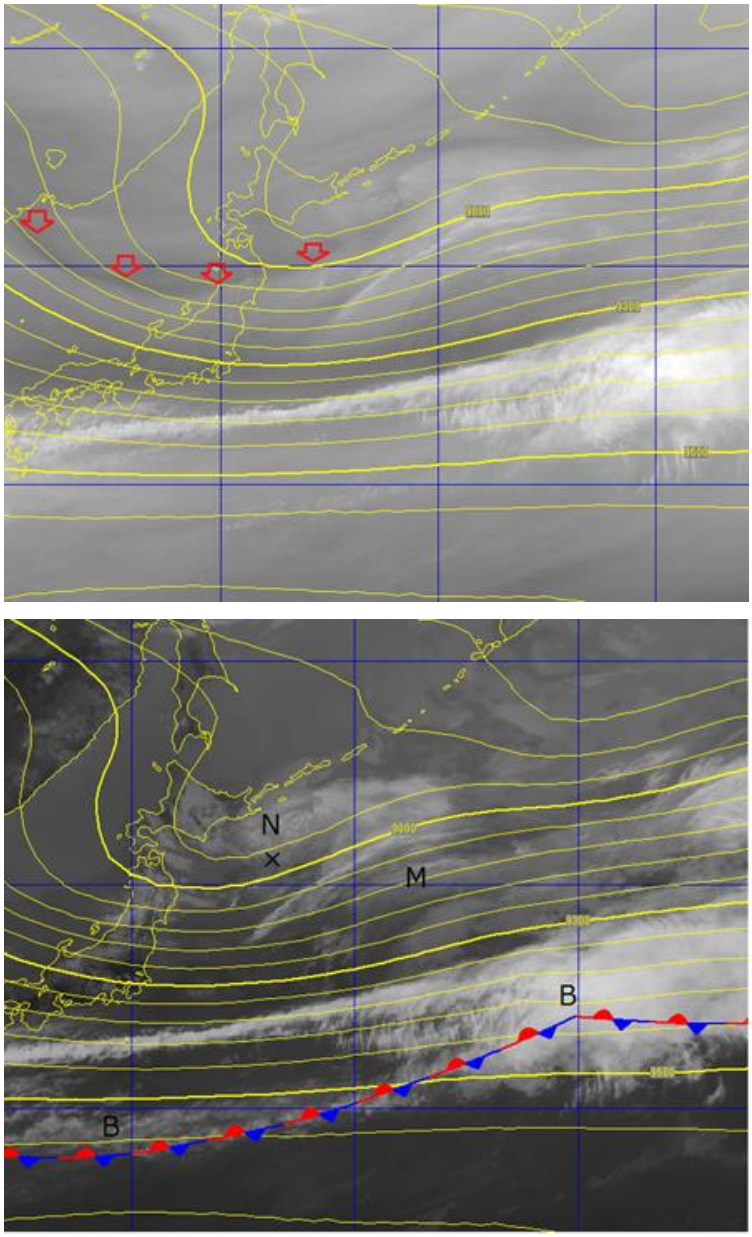

Fig. 5-2-22. Instant occlusion with development (MYB model), initial stage, at 06:00 UTC on 10 May 2015. Top: B10 water vapor image with 300-hPa isohypse and arrows marking the boundary; bottom: B13 infrared image

2. Occlusion Commencement Stage (Fig. 5-2-23)

The comma cloud **N** and the cloud area off the Sanriku coast **M** start to merge here. **N** has a higher cloud top with anticyclonic curvature at its northern edge, demonstrating development. Toward the south of **N**, the frontal cloud band top height also increases, bringing an occlusion pattern where the two cloud areas come into contact. The comma cloud and the cloud band represent cyclonic conditions with a front and a stationary front, respectively. This pre-occlusion state is indicated by the incomplete connection between the two cloud types and by

the relatively minor anticyclonic curvature of the cloud band.

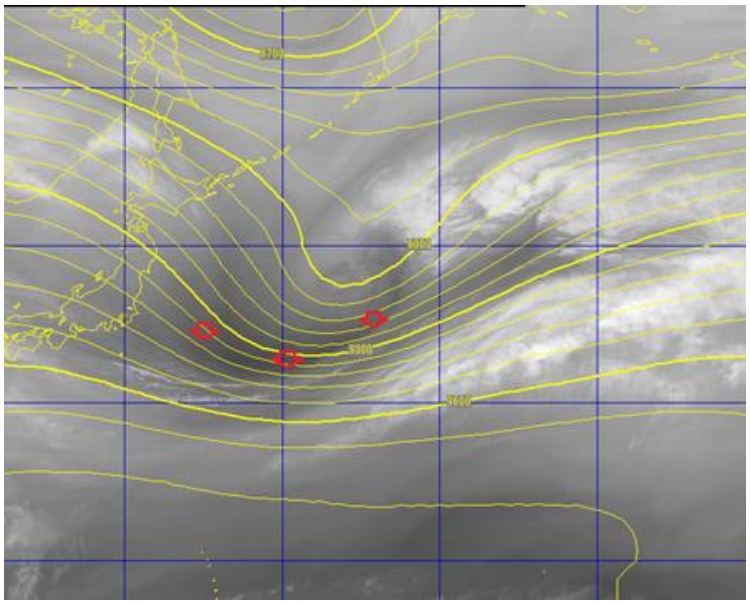

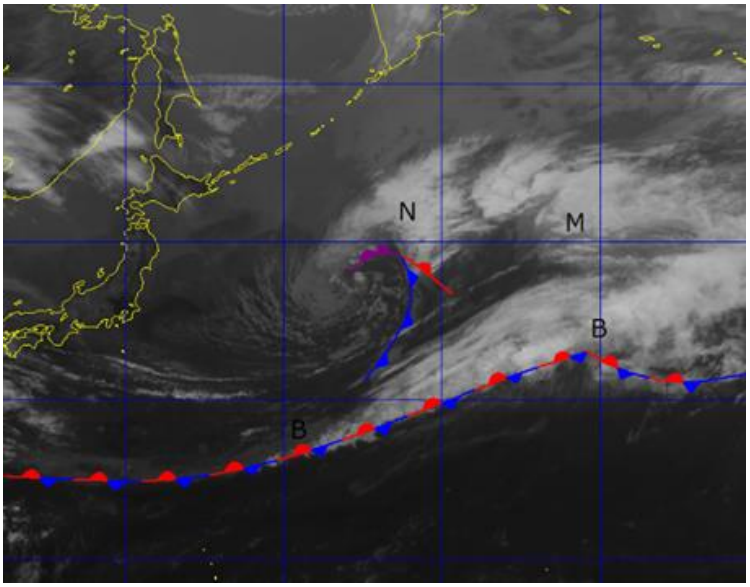

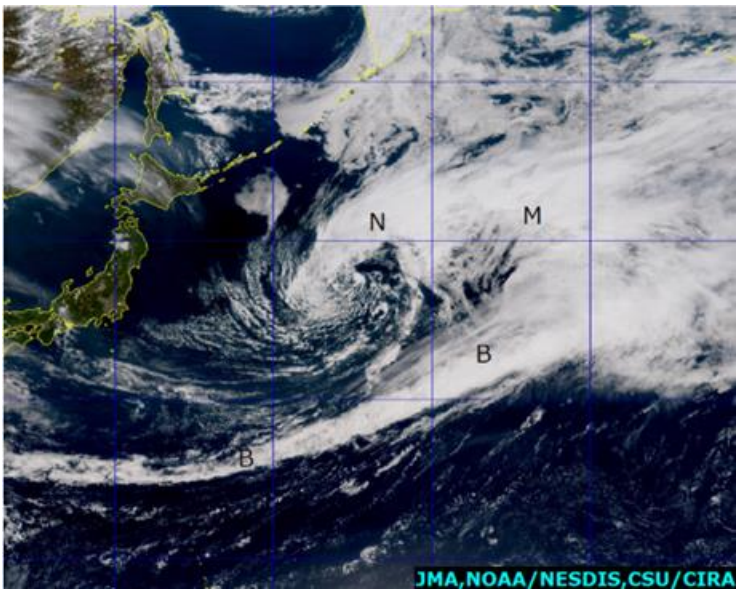

Fig. 5-2-23. Instant occlusion with development (MYB model), occlusion commenced, at 00:00 UTC on 11 May 2015. Top: B10 water vapor image with 300-hPa isohypse and arrows marking the boundary; middle: B13 infrared image; bottom: True Color Reproduction image

3. Occlusion Completion Stage (Fig. 5-2-24)

The cloud top is raised where the frontal cloud band and the comma cloud merge. The anticyclonic curvature **F-F** is distinct at the northern edge of the cloud band, and a dry slot **D** is also seen, indicating completion of the occlusion. The cyclone then follows the pattern of the standard mature stage.

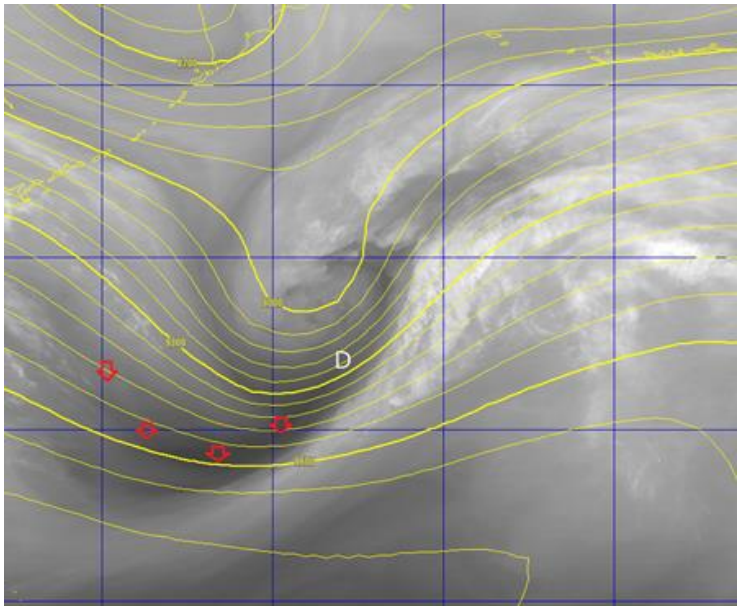

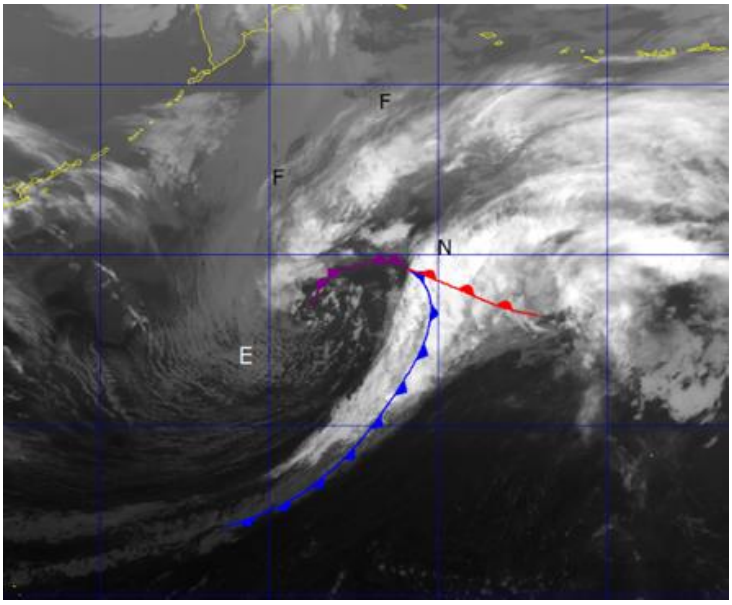

Fig. 5-2-24. Instant occlusion with development (MYB model), occlusion completed, at 12:00 UTC on 11 May 2015. Top: B10 water vapor image with 300-hPa isohypse and arrows marking the boundary; bottom: B13 infrared image

5.2.4. T-bone-type Development

The cyclonic development model presented by Shapiro and Keyser (1990; referred to here as the SK model) differs from the Bjerknes model (Fig. 5-2-25) in that a cold front does not join a warm front (i.e., frontal fracture). At the cyclonic center, cold air to the rear does not cover the surface (i.e., forming an occlusion), but a warm core remains behind (i.e., forming a warm-core seclusion). A warm front extends to the rear westward of the cyclonic center (i.e., forming a backward-arching warm front), but does not represent an occluded front.

A characteristic T-bone (i.e., T-shaped) cloud pattern, seemingly applicable to the SK model, resembling a warm occlusion is often seen in satellite imagery. A cyclone with this T-bone formation is described here for analysis in the context of the SK model, which does not explain all aspects of cyclonic development and structure. For instance, regarding backward-arching warm fronts, various discussions have been held on warm-front structures extending to the rear of cyclones. As with the warm-core seclusion period, analysis of multi-layer fronts entwined with the cyclonic center remains problematic. In contrast, satellite imagery for frontal fractures and warm core seclusions tends to match objective analysis for temperature fields and other variables.

In the SK model, in-depth analysis of mesoscale structures with insight is necessary, but weather charts and satellite imagery do not necessarily offer comprehensive details. This model may require consideration regarding applicability to weather chart analysis because of its limitations.

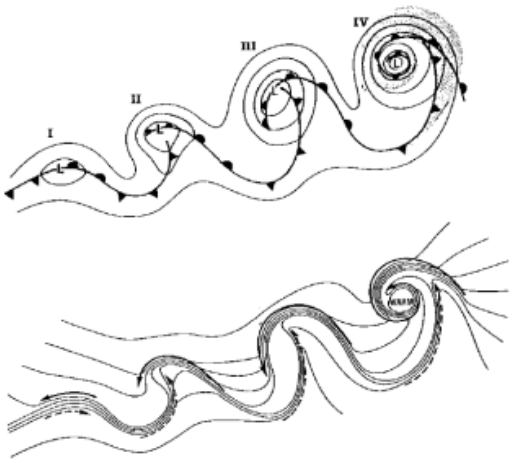

Fig. 5-2-25. T-bone models (Shapiro and Keyser, 1990)
I: incipient frontal cyclone; II: frontal fracture; III: backward-arching warm front and T-bone; IV: warm-core frontal seclusion
Top: isohypse (solid line), cloud area (dotted); bottom: temperature (solid lines), cold-air current (solid lines with arrow heads), warm-air current (dashed lines with arrow heads)

1. Initial Stage (Fig. 5-2-26)

A bulging cloud area here advances east-northeastward east of Japan with a pattern and characteristics similar to those seen the early-development stage of the standard type.

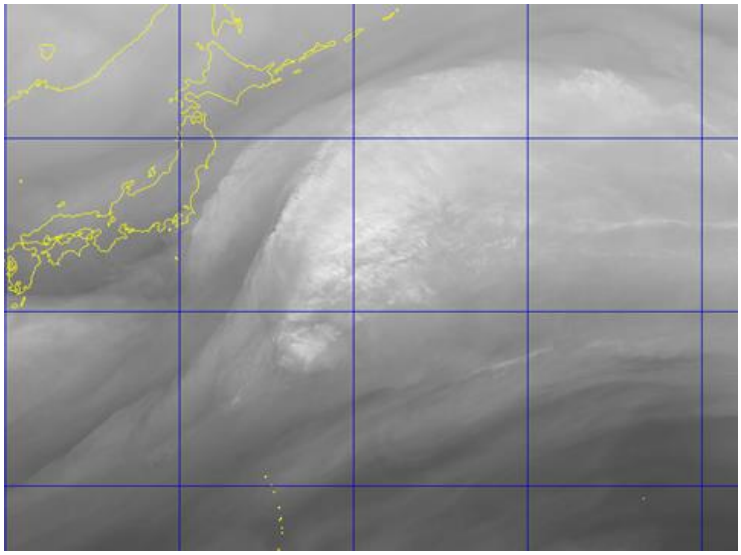

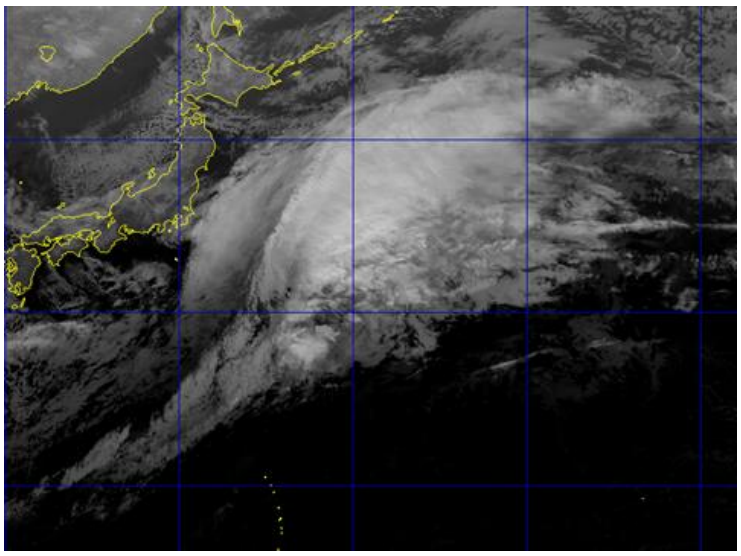

Fig. 5-2-26. T-bone development, initial stage, at 18:00 UTC on 6 February 2016
Top: B10 water vapor image; bottom: B13 infrared image

2. Frontal Fracture (Fig. 5-2-27)

The cloud area advancing east-northeastward to the east of Japan here has a further area extending east-westward, in contrast to the standard type. Anticyclonic curvature is increased at the northern edge, with a cloudless region intruding from the west. A notch (marked with arrows) begins to form, enabling determination of the cyclonic center. Although this resembles a warm occlusion pattern in the imagery, objective analysis at 850 hPa indicates no southward descent, meaning that the occlusion process has not started. A warm front is seen at the southern edge of the low-cloud area. The band C-C with convective clouds corresponding to the cold front extends southwestward, intersecting almost perpendicularly with the cloud area corresponding to the warm front extending longitudinally. In objective analysis at 850 hPa, cold advection intensifies at C-C, exhibiting a distinct cold-front structure. In contrast, the structure of the front farther north is unclear. The cold front exhibits a decreased temperature gradient at the region in contact with the warm front, as with the frontal-fracture structure in the SK model. In satellite imagery, the fractured and non-fractured parts are hard to distinguish.

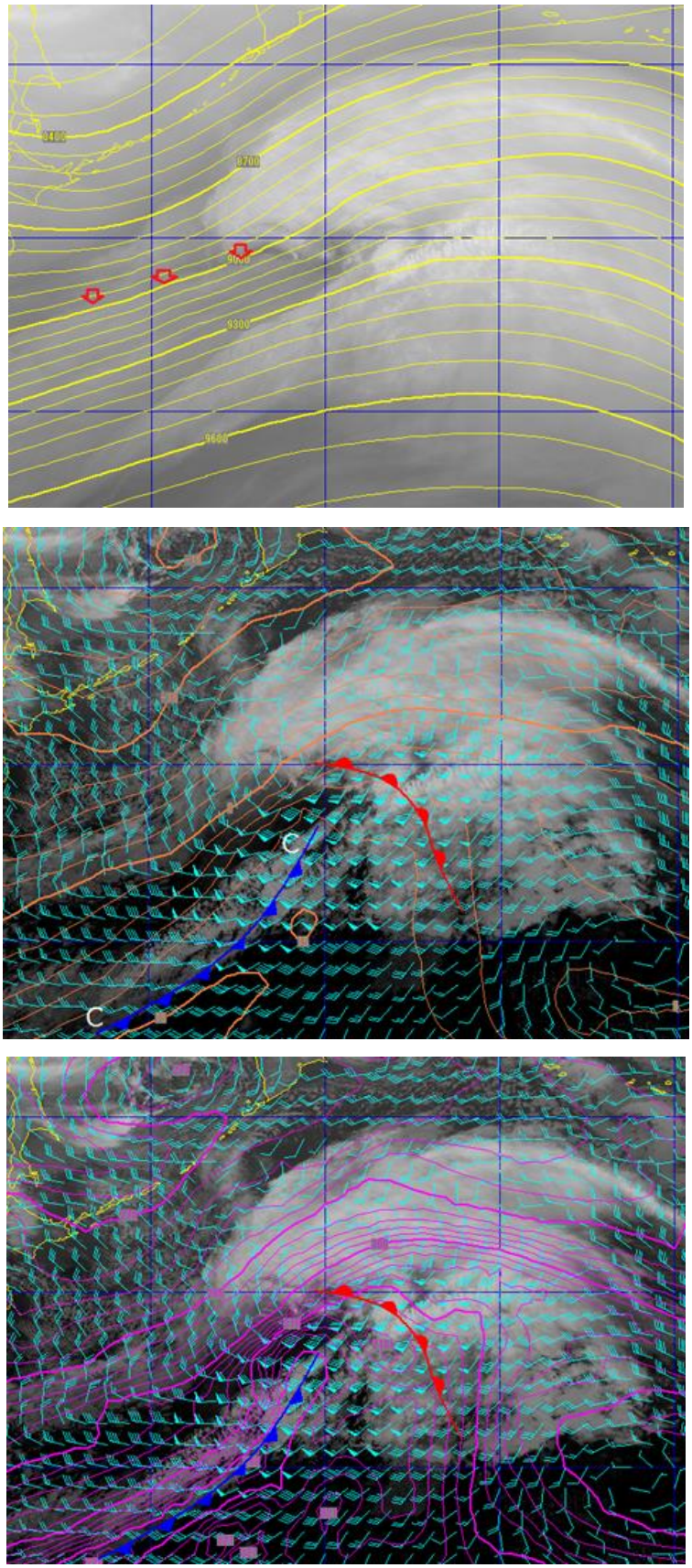

Fig. 5-2-27. T-bone development, frontal fracture, at 06:00 UTC on 7 February 2016
Top: B10 water vapor image with 300-hPa isohypse and arrows marking the boundary; middle: B13 infrared image, wind and temperature at 850 hPa; bottom: B13 infrared image,

wind and equivalent potential temperature at 850 hPa (unseen in visible image)

3. Backward-arching Warm Front (Fig. 5-2-28)

A cloud area associated with a cyclone advances eastward to the Kuril Islands here. The tall cloud area **L-M-N** relative to the warm front extends from east to west, almost perpendicularly intersecting a cloud band corresponding to the cold front extending southward, to form a clear T-bone shape. A distinct warm-front structure is visible from objective analysis at 850 hPa temperature and equivalent potential in **L-M-N**. The low-cloud vortex seen to the south near **N** in the satellite imagery indicates a nearby cyclonic center. In the SK model, the backward-arching warm front is at the southern edge of the cloud area between **M** and **N**, or at the eastern edge of the low cloud area **N-P** extending farther southward from **N**. As these areas extend around the cyclonic center anticlockwise with cold air, the structure is more of a backward-arching cold front rather than a warm one. In the SK model, the cyclonic center is seen around **M**, crossing the warm front extending from the fractured cold front. However, cyclonic centers are rarely observed in this region, more frequently appearing where lower vortices are seen (around **N** to the west of the cross point **M**).

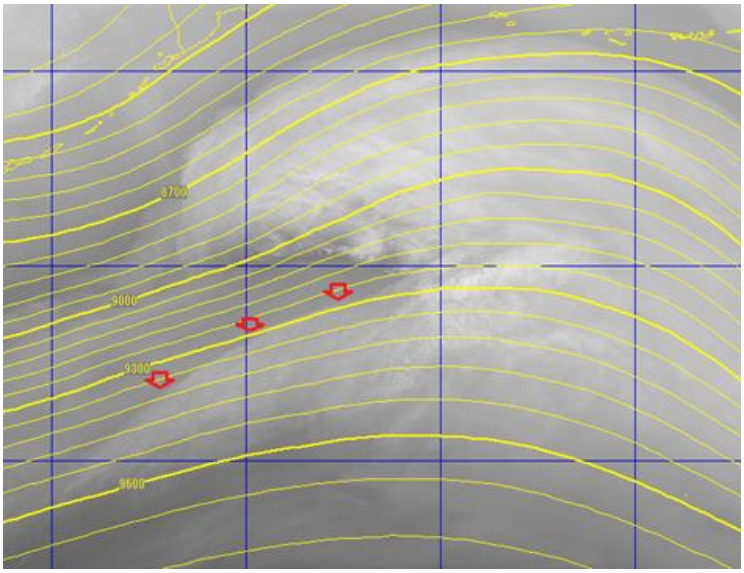

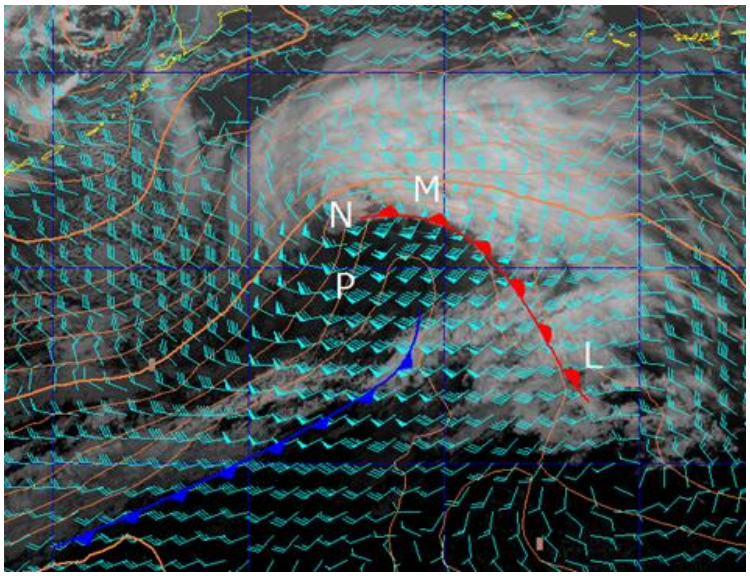

Fig. 5-2-28. Backward-arching warm front at 12:00 UTC on 7 February 2016
Top: B10 water vapor image with 300-hPa isohypse and arrows marking the boundary;
bottom: B13 infrared image, wind and temperature at 850 hPa

4. Warm-core Seclusion (Fig. 5-2-29)

In this satellite imagery, anticyclonic curvature becomes distinct at the northern and western edges of cloud areas. A low cloud vortex is also distinct here, with a dry slot around it indicating a cyclonic pattern resembling an occlusion. The cloud area starts to show meridional elongation on a course different from previous tendencies, with a cold-front cloud band extending southward across another cloud band north of a warm front to form a T-bone pattern. The low cloud vortex corresponds to the cyclonic center **L**.

In the SK model, this pattern is considered to indicate the progress of warm-core seclusion. A warm front can be identified in the figure at the edge of the cloud around the center. No clear warm core is observed at the isotherm of the 850 hPa weather map, but one can be determined from equivalent potential temperature.

Cold advection is stronger at **C** away from the center, leaving a relatively warm core around the center. In satellite imagery, a low-cloud vortex consisting of Cu and Sc represents the warm core. These clouds exhibit weak convective activity in contrast to cell-form convective clouds formed by cold-air intrusion, plausibly suggesting the presence of air relatively warmer than the surroundings.

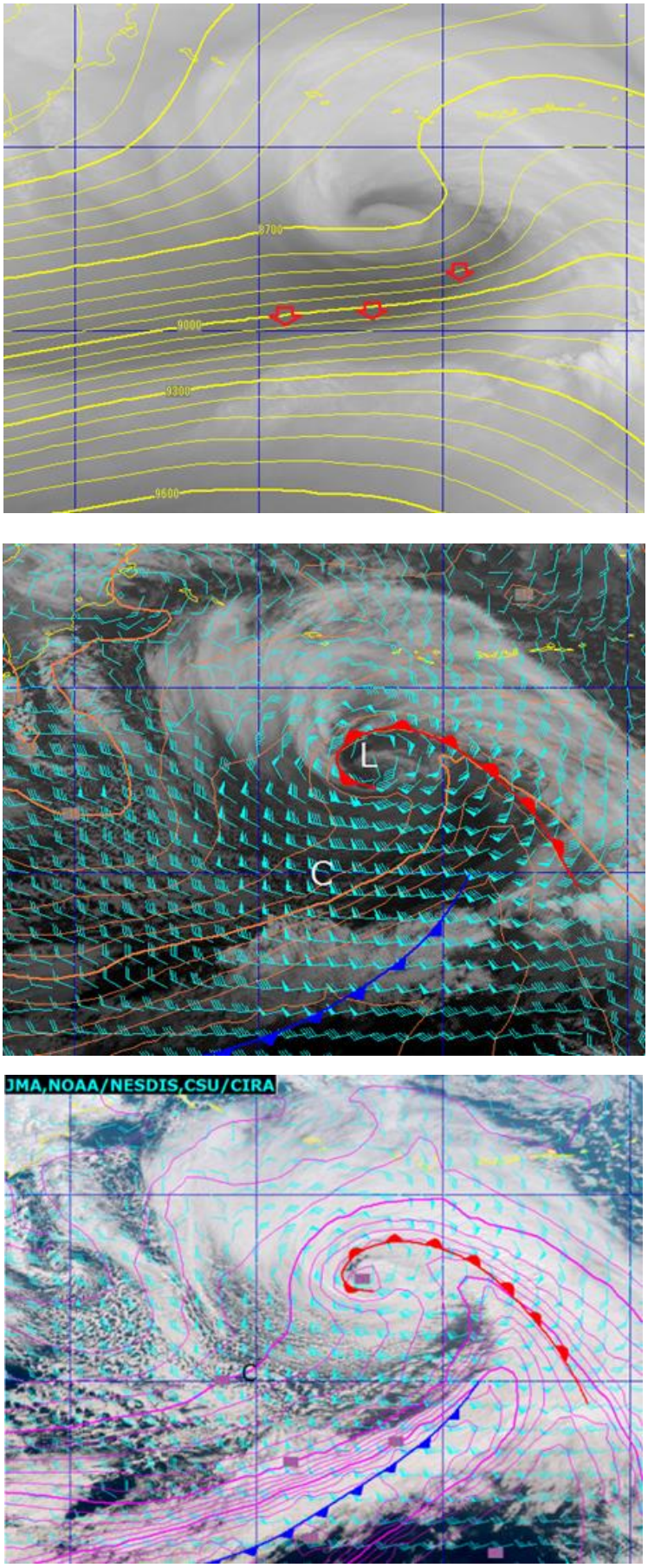

Fig. 5-2-29. Warm-core seclusion at 00:00 UTC on 8 February 2016

Top: B10 water vapor image with 300-hPa isohypse and arrows marking the boundary; middle: B13 infrared image, wind and temperature at 850 hPa; bottom: True Color Reproduction image, wind and equivalent potential temperature at 850 hPa